nature portfolio

https://doi.org/10.1038/s41586-023-05763-9

Supplementary information

Photosynthesis re-wired on the pico-second timescale

In the format provided by the authors and unedited

Supplementary information for

Photosynthesis re-wired on the pico-second timescale

Tomi K. Baikie[1,7], Laura T. Wey[2,3,7], Joshua M. Lawrence[2,4], Hitesh Medipally[5], Erwin Reisner[4], Marc M. Nowaczyk[5,6], Richard H. Friend[1], Christopher J. Howe[2*], Christoph Schnedermann[1*], Akshay Rao[1*], Jenny Z. Zhang[4*]

1- Laboratory, University of Cambridge, J. J. Thomson Avenue, Cambridge, CB3 0HE, UK
2 - Department of Biochemistry, University of Cambridge, Tennis Court Road, Cambridge, CB2 1QW, UK
3 - Department of Life Technologies, University of Turku, Turku, Finland.
4 - Yusuf Hamied Department of Chemistry, University of Cambridge, Lensfield Road, Cambridge, CB1 2EW, UK
5 - Plant Biochemistry, Ruhr-Universität Bochum, Universitätsstrasse 150, 44780 Bochum, Germany
6 - Department of Biochemistry, University of Rostock, Albert-Einstein-Str. 3, 18059 Rostock, Germany
7 - These authors contributed equally: Tomi K. Baikie, Laura T. Wey

Table of Contents

Figures

Supplementary Information

1. Ultrafast Transient Absorption Spectroscopy

1.1. TA controls on wild-type cells

1.1.1. Samples not damaged over long laser illumination

Measurements were made over 15 min on average (maximum 17 min) and a fresh biological sample was loaded into the cuvette for each measurement. To check whether the photosystem reaction centres were degrading under the laser during these measurements, additional measurements were made whereby wild-type *Synechocystis* cells in solution were exposed to the laser continuously for 2 h. This is an 8-fold increase in duration compared to the typical measurement time for experiments reported throughout. We compared the 2 hour measurement with a 15 minute measurement and found them to be no different beyond measurement uncertainty (**SI Figure 1**). As the samples were not stirred during measurements, these results also suggest that thermally driven Brownian motion continuously moved cells outside the laser focus point, preventing any measurable burn of the sample over the 2 h tested. Addition of DCBQ (any concentration) resulted in an initial equilibration period (15 min), after which no difference could be detected in the transient absorption signal within 2 h.

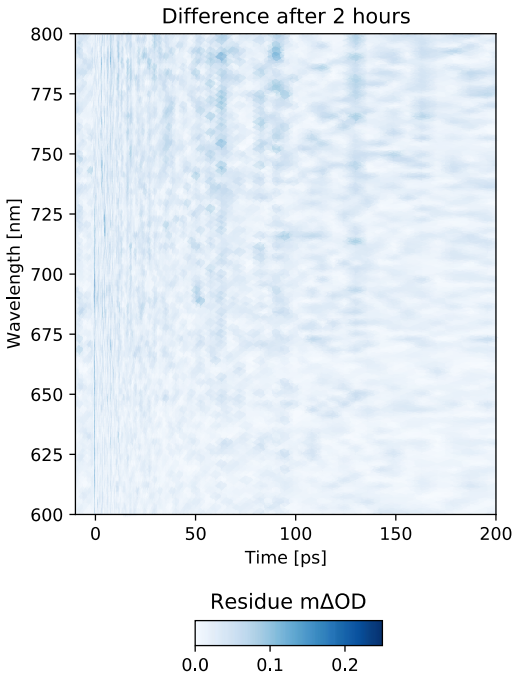

SI Figure 1 - Cell lifetime under laser illumination.
Difference between the ultrafast TA spectra from wild-type *Synechocystis* cells after a 15 minute measurement and after being exposed to the laser continuously for 2 h. No difference was observed, indicating that cells remained photoactive without appreciable changes in TA spectra. Difference map is of one biological sample, representative of multiple replicates (n = 3).

1.1.2. Agreement between biological replicates

For all TA experiments, biological replicates were collected for each biological sample. The number of biological replicates for each biological sample is specified in **SI Tables 3-12**. The spectral features of different biological replicates were in good agreement (**SI Figure 2**). A fit was completed using the global analysis method described below in **SI Section 1.4**. This gave us the confidence to present TA spectra from one biological sample representative of multiple biological replicates (e.g. **Figure 1D-E**, **Figure 3B**), and further quantitative analysis used multiple biological replicates as specified (e.g. **Figure 2C-D**, **Figure 3C**).

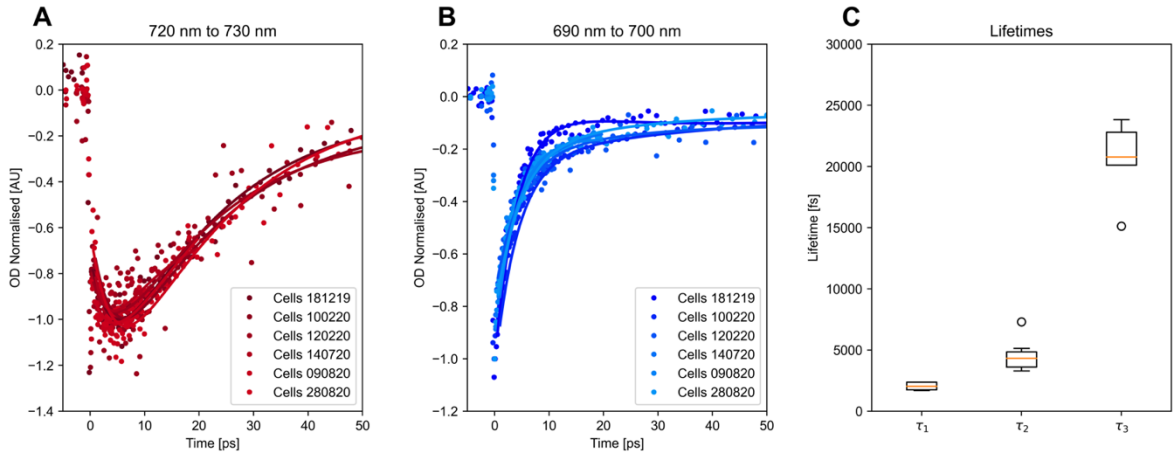

SI Figure 2 - Cell replicates.
A) The normalised averaged absorption signal between 720 nm and 730 nm, normalised at the peak of the rise at 8 ps, for six biological replicates of wild-type *Synechocystis* cells, with the date of the experiment (DDMMYY) over a period of 8 months. **B**) The averaged spectra between 690 nm and 700 nm normalised at 400 fs, avoiding the coherent artefact. Overlaid to the data points is the solid line fit based on the global fitting method. **C**) Lifetimes determined from the fit, revealing that the cells from different replicate cultures display remarkable consistency in the decay constant.

1.1.3. No damage or sub populations measured with increasing laser power

We investigated whether the transient absorbance signal exhibited linear or non-linear effects with respect to the laser (pump) power. Non-linear behaviour could indicate damage to the photosystems or some population dependent process. Spectra of wild-type *Synechocystis* cells were measured over different laser powers between 0.25 - 0.40 mW at 450 nm (laser beam diameter 280 x 240 µm = 6.27 x 10^{-8} m^2, 370 - 600 mW cm^{-2}, 14000 - 22000 $\mu mol_{photons}$ m^{-2} s^{-1}). Spectra at 660 nm and 700 nm were extracted and integrated in time. As the power was varied from low energy to high energy, the dependence of the integrated transient absorption signal at 660 nm and 700 nm was shown to be linear, suggesting little degradation at these measurement powers and timescales (**SI Figure 3**).

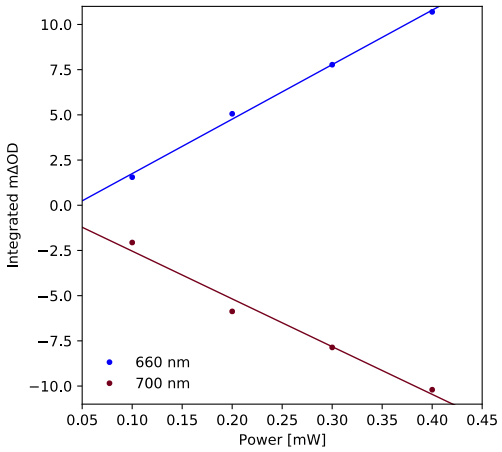

SI Figure 3 - Power dependence.
The integrated transient absorption signal against pump power at 450 nm. The brown line gives the integrated absorption at 700 nm, whereas the blue line gives the integrated absorption at 660 nm, which correlate to two wavelengths of opposing signal sign. In both the high energy and low energy datasets, the power dependence is linear against integrated mΔOD. This suggests a linear relationship between photon and RC interaction at time ranges >200 ps. All measurements reported elsewhere throughout this paper were made at 0.25 mW.

1.1.4. Determination that reactions centres are in a closed state during TA

Reaction centres can be considered in an open or closed state. For instance, in PSII an open reaction centre has the primary quinone Q_A oxidized and ready to undergo stable charge separation, whereas a closed reaction centre has Q_A reduced to Q_A^- and charge separation will be followed by fast charge recombination.[1] To characterise whether the reaction centres were in an open or closed state under the TA set-up, the spectra of wild-type *Synechocystis* cells were measured with and without constant illumination with a backlight intended to close the reaction centres. The spectra without and with the backlight were compared and found to be no different beyond measurement uncertainty (**SI Figure 4**). This indicated that the reaction centres were in a closed state during our measurements.

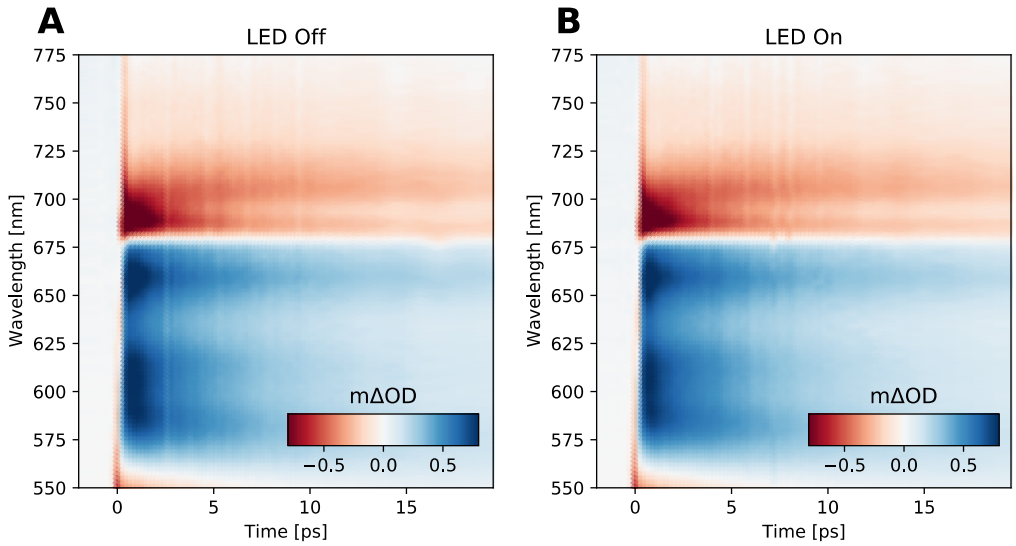

SI Figure 4 – Reaction centres within wild-type *Synechocystis* cells are closed during TA measurements. Ultrafast transient absorbance measurements were performed as previously reported.[2] The pump pulse was set to 450 nm. The sample solutions were placed in 1 mm path length cuvettes (Hellma). The pump and probe beams were focused to a size of $280 \times 240\ \mu m$ and $55 \times 67\ \mu m$, respectively **A**) with no continuous illumination, and **B**) with a 1500 $\mu mol_{photons}\ m^{-2}\ s^{-1}$ white (520 - 900 nm) light LED pointing towards the sample and 10 cm from the laser overlap point during measurements. Maps are of one biological sample, representative of multiple replicates (n = 3).

1.1.5. Wavelength dependence

To investigate the behaviour of the spectral features, the wavelength of the pump pulse was varied. The first spectral feature of note centred around 680 nm that formed within 200 fs of photoexcitation, which we assigned to a highly delocalised intermediate charge-transfer (CT) state. This feature was present in the spectra measured from photoexcitation of wild-type *Synechocystis* cells with a 200 fs pump pulse centred at 405 nm, 450 nm and 470 nm (**SI Figure 5A-C**). The feature centred around 680 nm was not as readily observed in the spectra measured with a pump pulse centred at 550 nm, which corresponds to the lack of absorption features in the steady state absorption spectra at 550 nm (**SI Figure 5D**) and was obscured with the pump pulse centred at 600 nm and 680, over which a white overlay has been applied (**SI Figure 5E-F**). Another spectral feature, centred around 715 nm, grows in within ~2 ps after photoexcitation and subsequently decays on a longer ps timescale, which we assigned to rapid excited state relaxation processes within the reaction centres. This feature was present in the spectra measured with a pump pulse centred at 405 nm, 450 nm, 470 nm, 550 nm and 680 nm (**SI Figure 5A-D** & **F**). For all other measurements, a pump pulse centred at 450 nm was chosen, because of its high absorbance by the sample, and clarity in the 525-725 nm region. With the 680 nm pump we also added 5 mM DCBQ to the cell sample (**SI Figure 6C**), to evidence that DCBQ mediated electron transfer need not invoke higher excited states beyond band edge excitation.

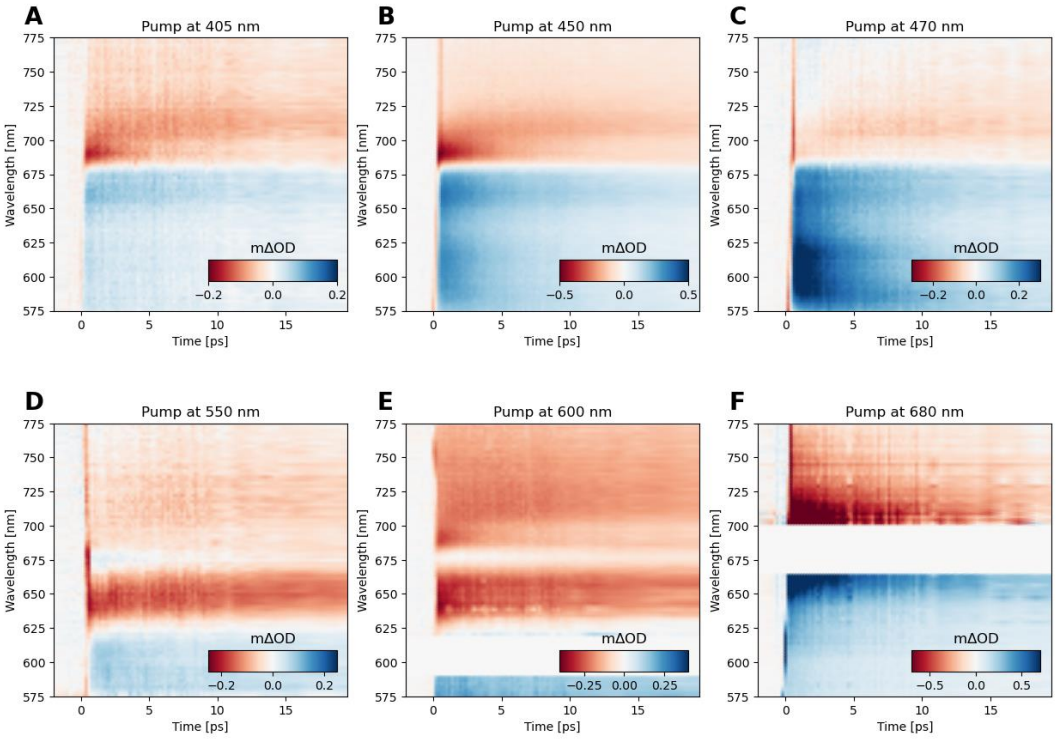

SI Figure 5 - Wavelength dependence in transient absorbance experiments.
Ultrafast transient absorption spectra of wild-type *Synechocystis* cells with different wavelengths of the pump pulse. One sample is shown for each pump pulse wavelength, representative of three biological replicates measured.

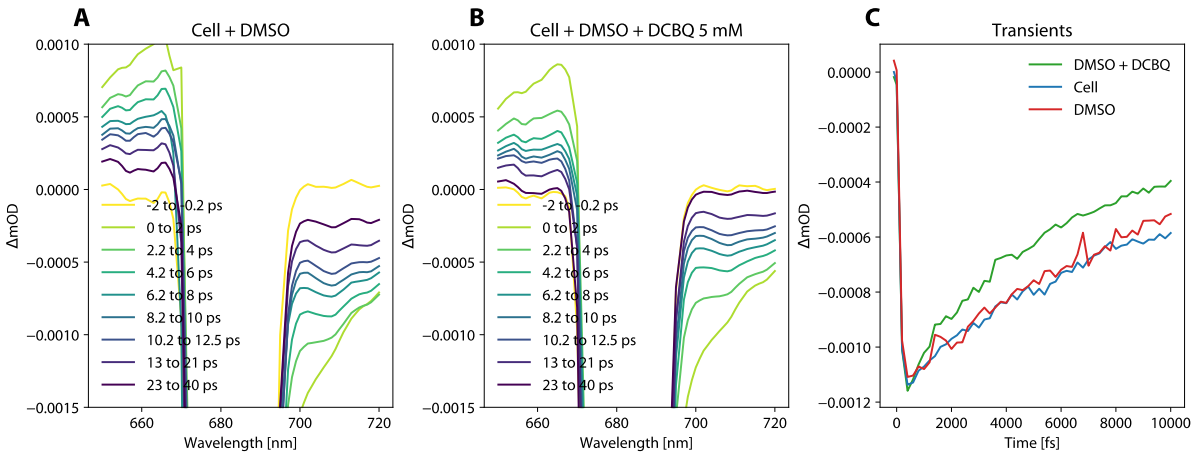

SI Figure 6 - TA spectra and DCBQ mediated accelerated decay dynamics at 680 nm pump experiments.
A Spectra from cells and DMSO (5%) excited at 680 nm. **B** Spectra from cells, DCBQ (5 mM) in DMSO (5%) excited at 680 nm. The supressed rise at 710 nm is visible. **C** – Cell (in blue), plus DMSO (in red) and DMSO and DCBQ (in green) transients, averaged between 708 and 715 nm, plotted as a function of time, highlighting the DCBQ induced accelerated decay.

1.2. Introducing the different biological samples and their TA spectra

To help assign the transient spectral features of wild-type *Synechocystis* cells to the different components in the PETC, different biological samples were tested: isolated PSII dimers,[3] isolated PSI monomers,[4] mutant *Synechocystis* cells lacking intact PSI complexes but with intact PSII complexes (PSI-less cells),[5] mutant *Synechocystis* cells lacking intact PSII complexes but with intact PSI complexes (PSII-less cells),[6] and the Olive mutant which has no phycocyanin (PC) discs but still has the allophycocyanin (APC) core of the phycobilisome (PBS).[7] Each biological sample was loaded into the cuvette at a final concentration of 5 $nmol_{Chl}$ ml^{-1}, and excited with a 200 fs pump pulse centred at 450 nm.

The spectra of PSII-less cells (**SI Figure 7 B**) appeared closer to that of wild-type cells (**Figure 1D**, **SI Figure 7A**), with the familiar low-energy spectral feature >690 nm and a zero-signal crossing at 682 nm at 400 fs. The spectra of isolated PSI (**SI Figure 7E**) was consistent with previous studies and contained the low-energy spectral feature >690 nm.[8]

In contrast, the spectra of PSI-less cells (**SI Figure 7C**) showed a wealth of spectral features that were markedly different from wild-type cells and similar to the spectra of isolated PSII (**SI Figure 7F**). The transient absorption spectra of isolated PSII were consistent with previous studies.[8] Notably, in the spectra of PSI-less cells and isolated PSII there was a very long-lived positive signal (i.e. less absorption) at its absorption maximum at 680 nm that lasted longer than a nanosecond.

TA spectrum of Olive mutant cells was similar to wild-type cells, indicating that the PC discs in the PBS were not responsible for the features in the visible range when illuminated at 450 nm (**SI Figure 7D**). A mutant with the entire PBS removed including the APC core could be investigated in future studies to further probe the nature of the AC core on the high energy (< 650 nm) bleach signal. Part of the bleach at < 650 nm may be attributed to non-photosystem photoactive components of cells, such as complete PBS containing the AC core and carotenoids. Therefore, in our analysis of the photodynamics of the photosystems, we focus on the lower energy features around 685 and 715 nm, which assign to different components in the PETC and are supported by isolated reaction centre studies (**SI Figure 7E-F**).

From the results of all these different biological samples, the transient spectral features of wild-type *Synechocystis* cells could be assigned to the different components in the PETC. The feature centred around 715 nm was present only in the spectra of wild-type and PSII-less cells, hence we conclude that PSI action is responsible for this feature, which we show is readily quenched by the action of DCBQ. Long-lived features were present in the spectra of isolated PSII and the PSI-less cells, so were assigned to PSII action. We note that the 685 feature is a combination of PSI and PSII signals in the cells and any system with both PSI and PSII, rendering unambiguous assignment difficult

The wild-type cells' initial transient spectral features were dominated by signatures from PSI, as might be expected based on a PSI trimer having approximately 4-fold higher chlorophyll count compared to a PSII dimer and an assumption that there existed an equal number of PSII dimers to PSI trimers per complete PETC in wild-type cells.[9] Similarly, the PSI-less cells had a lower signal intensity and signal to noise ratio with lower chlorophyll content for similar cell size (scattering), making it a challenging sample for absorbance spectroscopy.

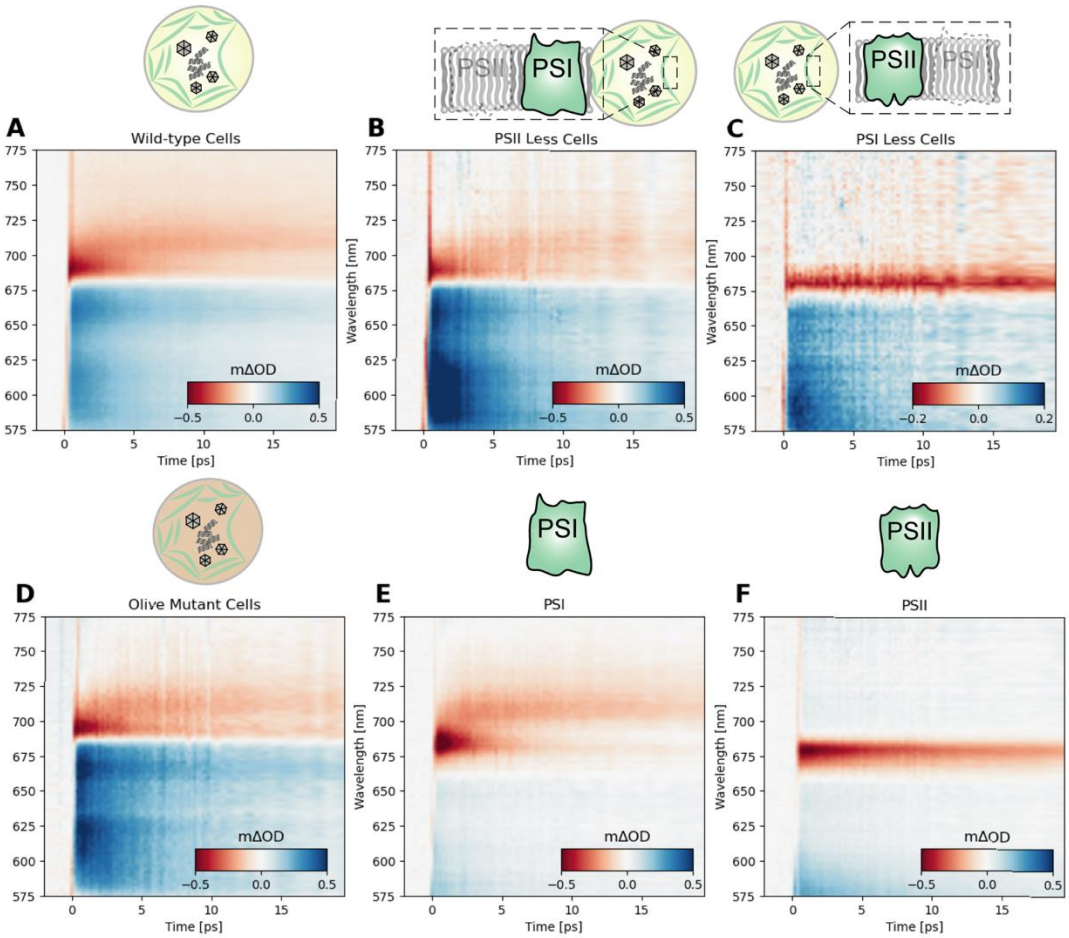

SI Figure 7 - TA comparison between biological samples

Ultrafast transient absorption spectra of different biological samples. **A)** *Synechocystis* cells wild-type, **B**) photosystem I (PSI)-less mutant cells with only photosystem II (PSII), **C)** PSII-less mutant cells with only PSI; **D)** Olive mutant cells with no phycocyanin (PC) discs but still with the allophycocyanin (APC) core of the phycobilisomes (PBS) and **E)** Isolated PSI, and **F)** Isolated PSII. All biological samples were excited at 450 nm. One biological replicate shown for each sample, representative of three to six biological replicates measured.

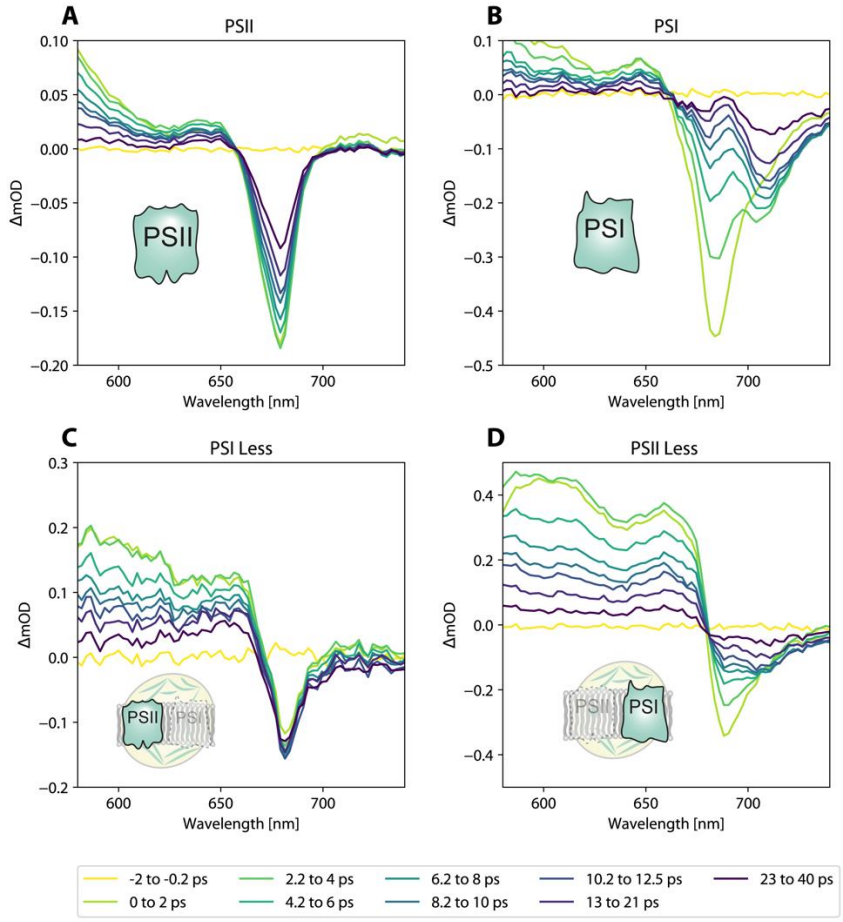

SI Figure 8 - TA spectral comparison between biological samples
Ultrafast transient absorption spectra at selected times of different biological samples. **A)** Isolated PSI, and **B)** Isolated PSII **C**) photosystem I (PSI)-less mutant cells with only photosystem II (PSII), **D)** PSII-less mutant cells with only PSI. All biological samples were excited at 450 nm. One biological replicate shown for each sample, representative of three to six biological replicates measured. Cell spectra with and without the presence of DMSO and DCBQ is given **SI Figure 13** – TA of wild-type *Synechocystis* cells in the presence of DCBQ and DMSO

1.3. PSI in previous studies

Although the spectral dynamics of isolated PSI in previous studies resemble our isolated PSI measurement, some differences remain in terms of the clarity and exact energy of the observed features. This would be expected given that PSI protein supercomplexes differ in different photosynthetic organisms (summarised in next paragraph) in terms of their light harvesting components, types of chlorophylls and absorption of different chlorophyll *a* pigments. Further, studies on isolated systems also involve different purification processes e.g. in membrane or particles, trimer or monomer, whole super complex or core. For these reasons we compare our whole cell wild-type and mutant spectra to our isolated PS spectra (all cyanobacterial systems, and all with the photosystems in their final complex form e.g. we use an isolated PSII dimer, PSI trimers).

In plants and algae, PSI is in a supercomplex of a core and a light-harvesting component (PSI-LHCI). In cyanobacteria, the phycobilisomes (PBS) are mainly an antennae for PSII but also for PSI during state transitions. Plant and algal PSI and associated light harvesting complexes also contain chlorophyll *b*, whereas cyanobacteria only contain chlorophyll *a*. There are other cyanobacterial species that contain

far red chlorophylls in their PSII like chlorophyll *d* and *f,*[10] but not in *Synechocystis*. Within the chlorophyll *a* pigments, there are "red forms", which absorb at lower energy than the reaction centre chlorophylls at wavelengths longer than 700 nm (more background and reviewed by Karapetyan et al., 2006 [11]). Red chlorophylls differ in number, position and absorption in PSI in different photosynthetic organisms. The number of red chlorophylls is very species dependent. 5-10% of the chlorophylls are far red in different cyanobacteria.[12] The red chlorophylls in plants are largely located in the peripheral LHCI complexes away from the P700.[13] However, in cyanobacteria these red chlorophylls are located in the core of PSI. In cyanobacteria, the most red forms are created in the edges of the monomers coming together in the PSI trimer.[14] In plants, the red chlorophylls absorb in the 710−730 nm window.[15] In cyanobacteria, the red chlorophylls are more diverse and absorb in the 705-740 nm region. In *Synechocystis* PSI (our whole cell species), the red Chls absorb in the 707-715 nm window.[16] In Thermo elongatus PSI trimers (our isolated PS species), the red Chls absorb in 708 and 719 nm.[14] *Spirulina platensis* has the most red shifted chlorophyll known with an absorption centred at 740 nm.[16]

Table 1 PSI and PSII literature comparison**Description of biological sample**	**Cyanobacteria or Algae/Plant**	**TA Pump Wavelength**	**Reference**
Partial (subunits A−E, K, and M) monomeric PSI complex from *Synechocystis* sp. PCC 6803	Cyanobacteria	680 nm	Akhtar et al., 2021 [17]
Trimeric PSI complexes from *Synechocystis sp.* PCC 6803	Cyanobacteria	720 nm	Shelaev et al., 2010 [18]
PSI trimers from *Synechocystis* sp. PCC 6803	Cyanobacteria	720 – 760 nm	Cherepanov et al., 2017 [19]
PSI in intact membranes, PSI in detergent-isolated particles from PSII-less *Synechocystis* sp. PCC 6803	Cyanobacteria	590 nm	Hastings et al., 1995 [20]
PSI complexes isolated from *Synechococcus* sp. PCC 7002 and *Synechocystis sp*. PCC 6803	Cyanobacteria	700 nm	Lee et al., 2018 [21]
Trimeric PSI of *Thermosynechococcus elongatus*	Cyanobacteria	675 nm	Anna et al., 2012 [22]
PSI core of *Spirulina platensis*	Cyanobacteria	680 nm	Russo et al., 2022 [16]
core PSI particles of *Chlamydomonas reinhardtii*	Algae/Plant	670 & 700 nm	Muller et al., 2003 [23]
detergent-isolated PSI core particles from *Chlamydomonas reinhardtii* (wild-type and with HN(B656) mutation in PSI)	Algae/Plant	590 nm	Melkozernov et al., 1997 [24]
isolated PSI-Light-Harvesting Complex I (PSI-LHCI) supercomplex and in the isolated PSI core complex of *Spinacia oleracea*	Algae/Plant	480 – 650 nm	Russo et al. 2020 [25]
PSI-LHCI supercomplex isolated from *Spinacia oleracea*	Algae/Plant	490 & 620 nm	Molotokaite et al., 2017 [15]

isolated core and intact PSI particles and stroma membranes from *Arabidopsis thaliana*	Algae/Plant	663 nm	Slavov et al., 2008 [26]
PSI–LHCI and PSI–LHCI–LHCII supercomplexes isolated from *Arabidopsis thaliana*	Algae/Plant	N/A (TCSPC)	Santabarbara et al., 2017 [27]
Proteoliposomes with native plant thylakoid membrane lipids and different stoichiometric ratios of LHCII:PSI(LHCI) from *Pisum sativum*	Algae/Plant	N/A (TSCPC)	Akhtar et al., 2016 [28]

1.4. Global analysis of TA spectra

1.4.1. Background to global fitting

A transient absorption dataset can be thought of as a matrix with each point assigned a spectral value and a time value[29]. This time value is the delay of the probe pulse relative to the pump pulse. This may be negative if the probe pulse arrives before pump. The spectral value is the magnitude of the signal at some wavelength resolution. In some circumstances, it is permissible to assume that the wavelength components decay with some rate, i.e. their magnitude of the spectra changes in time. This is to say that the data is separable into wavelength spectra with a corresponding time dependent decay.

The data can also be made simpler, or more properly defined as "reducing the dimensions of the data". Instead of dealing with every timepoint and every wavelength datapoint, we attempt to simplify the data into fewer dimensions. Dimensionality reduction is a treatment common in many forms of data analysis, for instance in image compression. A common way of doing so is singular value decomposition (SVD), which is a method of drawing out the major components of the data. We retain the components of the data which describe the vast majority of the data. We now more rigorously define our data treatment below.

Global analyses are well established techniques to identify components of transient spectral data.[29] We provide a brief overview of the techniques utilised here. Supposing the spectral components behave independently, and the response of the detector is linear with intensity, Beer's law states that the noise-free, time-resolved absorption spectrum is a superposition of component's absorption spectrum weighted by their concentration. Thus, the absorption spectrum, $\psi(t,\lambda)$ can be written as a superposition of the contributions of the n different bases:

$$\psi(t,\lambda) = \sum_{l=1}^{n} c_l(t)\varepsilon_l(\lambda)$$

Equation 1

where $c_l(t)$ and $\varepsilon_l(\lambda)$ denote, respectively, the concentration and spectrum of a component. Practically, our transient data is recorded as a regular array $w \times t$ matrix, $[D]$, where w is the number of wavelengths in each spectrum and t is the number of time delays at which spectra are obtained. Beer's law can then be simply expressed in matrix form as by the product of two matrices:

$$[\mathrm{D}] = [\mathrm{A}][\mathrm{C}]$$

Equation 2

where $[\mathrm{A}]$ is a $w \times n$ matrix containing the spectra of the n individual components in its columns, while [C] is an $n \times t$ matrix containing the time behaviour of the excited-state concentrations of the components in

its rows. Using singular value decomposition (SVD) it is possible to reduce the dimensionality of the problem as well as fitting to a noise-reduced subset of matrix D. If D is an $m \times n$ real matrix with $m > n$, then D can be written in the form:

$$\mathrm{D} = \mathrm{USV}^{\mathrm{T}}$$

Equation 3

We follow the notation used by the Mathematica language, where U has dimensions of $m \times m$, S has $m \times n$, and V has $n \times n$. In both systems, U and V are unitary, so that $\mathrm{U}^{\mathrm{T}}\mathrm{U} = \mathrm{I}$ and $\mathrm{V}^{\mathrm{T}}\mathrm{V} = \mathrm{I}$ (where the two identity matrices may have different dimensions). S has entries only along the diagonal, known as singular values. The weighted left singular vectors (wLSV) are given by US. Assuming separability, as in Equation 2, decomposing the transient data in this way has a physical interpretation: U is the unitary matrix of left singular vectors giving the temporal dependence of the signal, V^{T} is the unitary matrix giving the spectral dependence of the signal. However, the spectra themselves cannot be directly assigned to a specific photoactive component.

Retaining the number of wLSVs whose corresponding singular values are significantly larger than the rest is a good approximation for a sufficient number of bases to retain.[30] The number of bases chosen gives only an estimate of the number of orthogonal components appropriate to represent the data. The choice in basis makes no estimation of any underlying reaction scheme. In global analysis, we conduct a simultaneous analysis of multiple kinetic traces at different wavelengths to model our dataset, or a noise-reduced subset of the dataset described by the basis choice from SVD. The reduced data facilitates the interpretation of observed dynamics by reducing the dimensionality of the problem. In this type of analysis we have no *a priori* knowledge for a detailed kinetic model, so we target a minimally descriptive model lessening the risk of identification problems due to over parameterisation. However, in this case, the results from our analysis likely leads to an oversimplification of the data as we resolve the minimum number of physical processes required to describe the dataset. We assume a model of the sum of weighted exponentials:

$$\psi(t, \lambda) = \sum_{i} A_i(\lambda) \mathrm{e}^{-t/\tau_i}$$

Equation 4

where i corresponds to the size of the basis expansion used to describe the data, $A_i(\lambda)$ denotes the coefficient related to each wavelength and τ_i is the lifetime associated with each exponential decay.

1.4.2. Singular value decomposition of different biological samples

To analyse the features of the transient absorbance spectra of the photosystems *in vitro* and *in vivo*, the spectra of the different biological samples with varying photosystems (described in **SI Section 1.2,** not including the Olive mutant) were deconvoluted by Singular Value Decomposition (SVD) as described above in **SI Section 1.4.2**. The transient data were decomposed into two vector sets: vectors giving the spectral dependence of the dataset and vectors giving the temporal dependence of the dataset. The number of wLSVs whose corresponding singular values were significantly larger than the rest was retained for each: three vectors were retained for wild-type cells (**SI Figure 9**) and PSII-less cells (**SI Figure 10A-C**), and two vectors were retained for isolated PSI (**SI Figure 10D-F**), isolated PSII (**SI Figure 11D-F**) and PSI-less mutant cells (**SI Figure 11A-C**).

Although these choices of vectors in the SVD decomposition do not estimate the underlying reaction scheme or necessarily correspond to individual photoactive machineries, they give a lower bound to the number of observed physical processes. Corresponding components, similar both in the spectral and temporal decomposition, were observed in the SVD of the PS-less cells and the isolated photosystems. Comparing isolated PSI and PSII-less cells (**SI Figure 10**), and distinctly, isolated PSII and PSI-less cells (**SI Figure 11**) the component spectra (Left SVD – panels **B** & **E** in **SI Figure 10** & **9**) and component concentrations (Right SVD – panels **C** & **F** in **SI Figure 10** & **9**) have similar features in the region of interest (650 – 750nm) as well similar component decays in each case. This further reaffirms our supposition that in the cell systems we directly resolve the reaction centres *in vivo*.

To evidence the validity of the basis in the SVD decomposition, the vectors described in **SI Figure 9**, **SI Figure 10** and **SI Figure 11** were combined to reform spectra and compared to the original data (**SI Figure 12**).

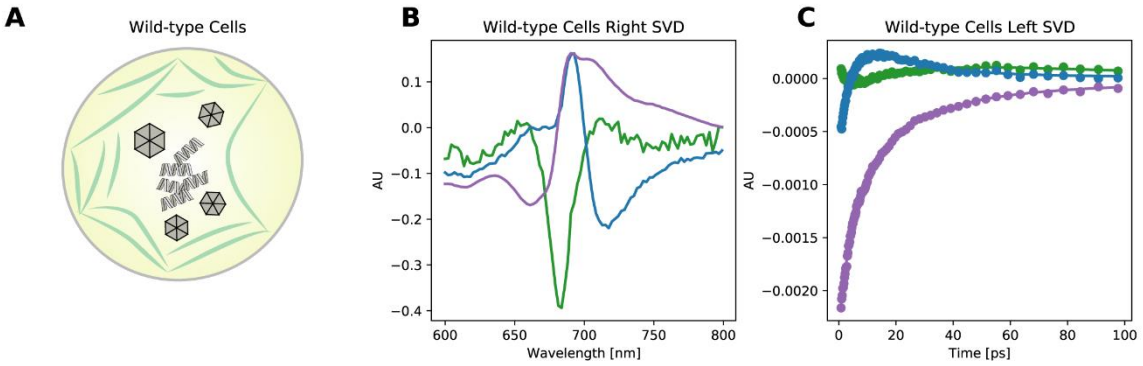

SI Figure 9 – Singular value decomposition (SVD) of the wild-type *Synechocystis* cells.
A) Cartoon of wild-type cells. **B**) Spectral dependence of the wild-type cells' TA data from SVD. SVD is an established method to decompose TA data, assuming the data is separable into spectral and wavelength components.[31] **C**) Corresponding temporal decay for spectral components from panel B. The SVD decomposition is given by solid round markers, and the global fit is the solid line in the corresponding colour. We roughly assign the green components to the bleach from PSII, whereas the blue and purple components are more difficult to allocate directly to a single reaction centre, however, they both include components from PSI. Data from one sample presented, which was representative of three biological replicates.

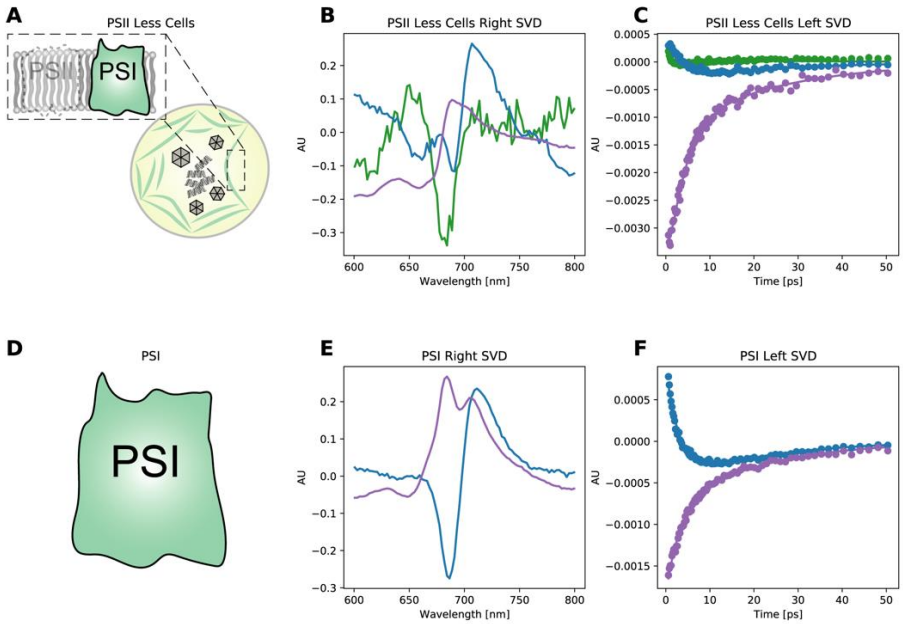

SI Figure 10 - Singular value decomposition (SVD) of mutant PSII-less cells and isolated PSI.
A) Cartoon of PSI-less cells. **B**) Spectral dependence of the PSI-less cells' TA data from SVD where 3 components were retained**.** SVD is an established method to decompose TA data**,** assuming the data is separable into spectral and wavelength components[31]. **C**) Corresponding temporal decay for spectral components from panel B. The SVD decomposition is given by solid round markers, and the global fit is the solid line in the corresponding colour. **D**) Cartoon of isolated PSI. **E**) Spectral dependence of the isolated PSI TA data from SVD where 2 components were retained. **F**) Corresponding temporal decay for spectral components from panel E. The SVD decomposition is given by solid round markers, and the global fit is the solid line in the corresponding colour. Data from one sample presented, which was representative of three biological replicates.

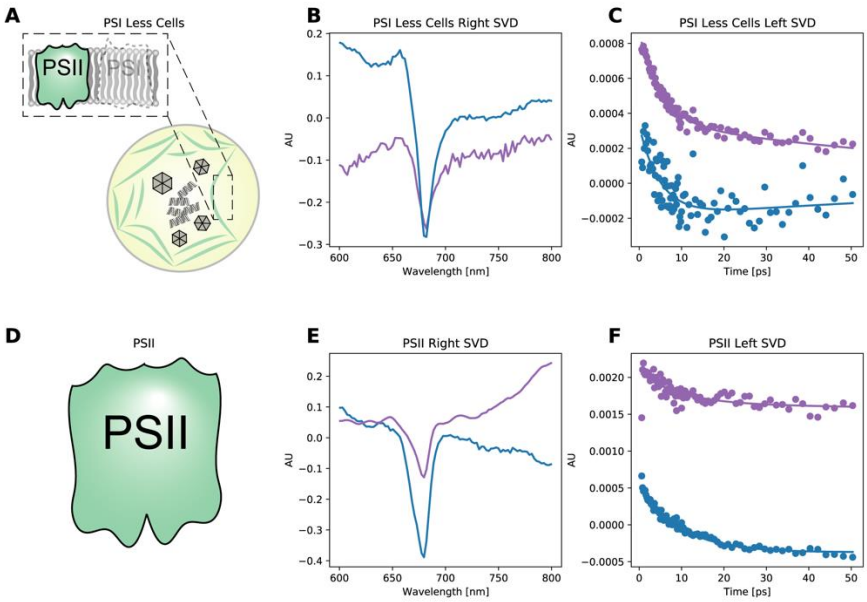

SI Figure 11 - Singular value decomposition (SVD) of mutant PSI-less cells and isolated PSII
A) Cartoon of PSII-less cells. **B**) Spectral dependence of the PSII-less cells' TA data from SVD with two components retained**.** SVD is an established method to decompose TA data**,** assuming the data is separable into spectral and wavelength components.[31] **C**) Corresponding temporal decay for spectral components from panel B. The SVD decomposition is given by solid round markers, and the global fit is the solid line in the corresponding colour. **D**) Cartoon of isolated PSII. **E**) Spectral dependence of the isolated PSI TA data from SVD with two components retained. **F**) Corresponding temporal decay for spectral components from panel E. The SVD decomposition is given by solid round markers, and the global fit is the solid line in the corresponding colour. Data from one sample presented, which was representative of three biological replicates.

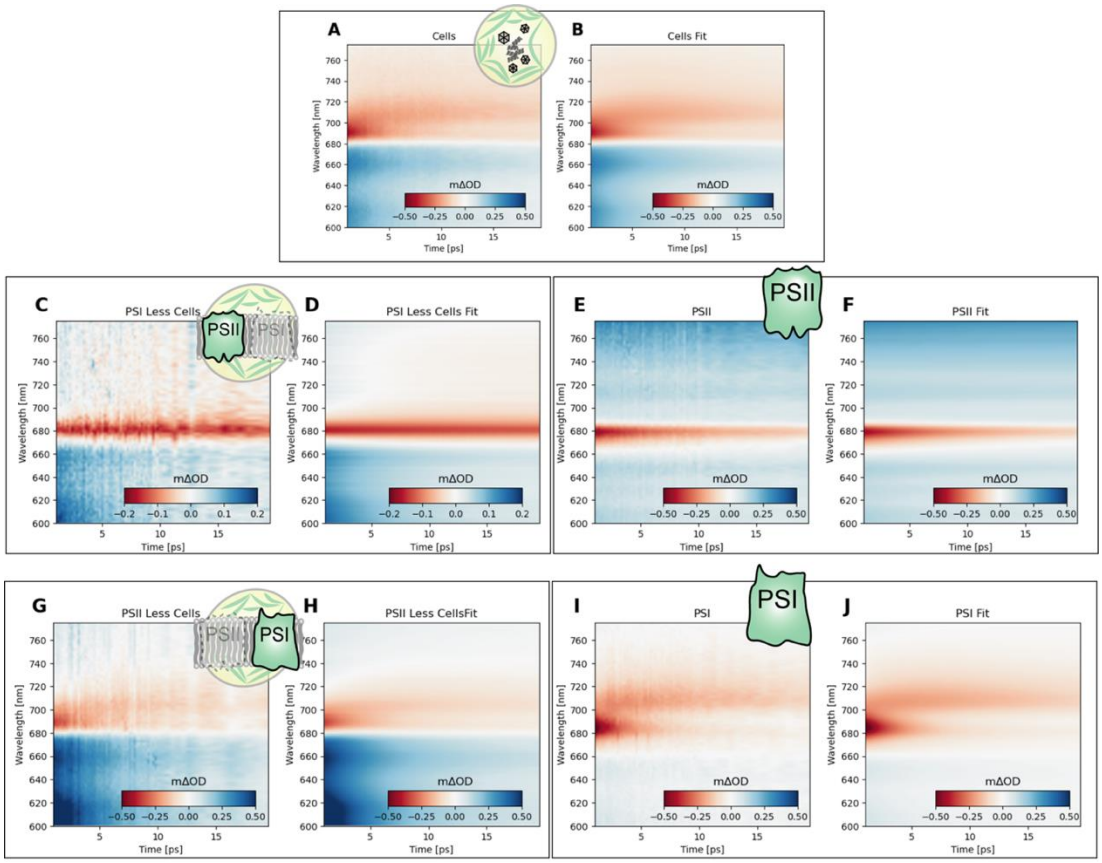

SI Figure 12 - Singular value decomposition summary.
Ultrafast TA spectra of different biological samples with varying photosystems: **A** & **B**) Wild-type cells, **C** & **D**) PSI-less cells, **E** & **F**) Isolated PSII, **G** & **H**) PSI-less cells and **I** & **J)** Isolated PSI. For each pairing, the spectra from TA measurements is given on the left, and the spectra reconstructed from the retained SVD components in SI Figure 9, SI Figure 10 and SI Figure 11 is given on the right. Data from one sample presented, which was representative of three biological replicates.

1.5. Addition of DCBQ to wild-type cells

1.5.1. TA spectral features of wild-type cells with DCBQ added

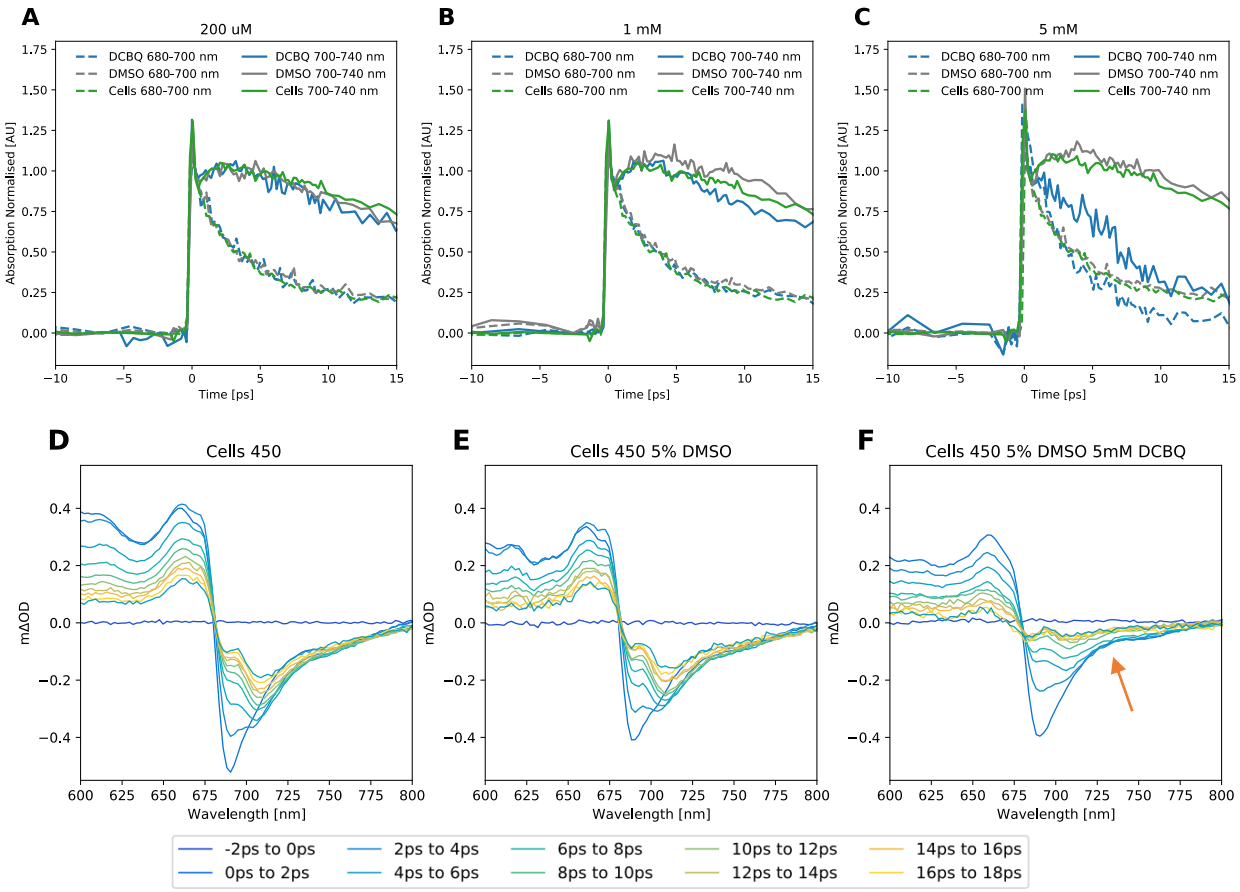

SI Figure 13 – TA of wild-type *Synechocystis* cells in the presence of DCBQ and DMSO
Wild-type cells (in green) have had an increasing volume of DMSO (in grey) and concentration of DCBQ + DMSO (blue) added, **A**) has 200 uM DCBQ added, which corresponds to 0.2% DMSO, **B**) has 1 mM DCBQ added, which corresponds to 1% DMSO, **C**) has 5 mM DCBQ added which corresponds to 5% DMSO. DMSO is the solvent by which DCBQ is solubilised, and so the effect of the DMSO can be determined. The effect of DMSO is small, even at high concentrations. Upon the addition of DCBQ, there is a dramatic decay in the 700nm to 740nm curve, which corresponds to the 715 nm feature in **D**, **E** and **F** and missing, as highlighted by the red arrow in **F**.

1.5.2. Model of DCBQ reduction by the reaction centre

Modelling the photosynthetic electron transport chain has been a subject of significant study.[29,32] For example, Müller *et al*. use nine distinct kinetic rates to describe the early electron transfer steps in isolated PSI.[33] Further, as experiments reported here were carried out at room temperature, the characteristic absorption spectra within the PETC broaden, which complicates the association of spectral features to specific elements in the PETC. In this study we cannot easily deconvolute these pathways, hence the use of the phenomenological model guided by the SVD component analysis in the preceding sections (**SI Section 1.4**). However, the global fitting method reported in **SI Section 1.4** is unable to describe branched models.

Based on our assessment described in the main text of the mechanism of DCBQ reduction by the highly delocalised CT state formed after the initial photoexcitation, we constructed a simple branched kinetic model (**SI Figure 12**), and use 3 distinct sequential states, which broadly correspond to the photoexcited reaction centres and electron acceptors (A_0 is the primary electron acceptor chlorophyll in PSI, pheophytin is the primary electron acceptor in PSII).

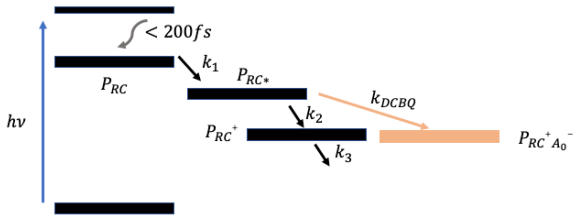

SI Figure 14 – Branched kinetic model of DCBQ reduction by the highly delocalised CT state formed after initial photoexcitation.
P_{RC} is the initially excited reaction centre (P680 in PSII or P700 in PSI), P_{RC^*} is a sequential state of the photoexcited reaction centre, $P_{RC^+DCBQ^-}$ is created upon reduction of DCBQ and P_{RC^+} is the natural decay pathway. k_1 (2 ps), k_2 (4.5 ps) and k_3 (20.8 ps) (see **SI Figure 2** - Cell replicates.) are the rate coefficients for the wild type cells.

Our branched kinetic model is defined by Equations 5 through 7,

$$\frac{dP_{RC}}{dt} = -k_1 P_{RC}$$

Equation 5

$$\frac{dP_{RC^*}}{dt} = k_1 P_{RC} - k_2 P_{RC^*} - k_{DCBQ} P_{RC^*}$$

Equation 6

$$\frac{dP_{RC^+A_0^-}}{dt} = k_2 P_{RC^*} - k_3 P_{RC^+A_0^-}$$

Equation 7

where P_{RC} is the photoexcited reaction centre (P680 in PSII or P700 in PSI), P_{RC^*} is a later photoexcited reaction centre (100% conversion efficiency from P_{RC}), P_{RC^+} is the final charge separate state and *t* is time. Attempts to globally fit the data with fewer rates did not yield satisfactory results.

1.5.3. Electron extraction efficiency as a function of DCBQ concentration

We utilise a compartmental model[29] to apply the proposed scheme in **SI Section 1.5.2** to the measured TA spectra. We carry out the analysis on a wild-type cell sample without DCBQ, where $k_{DCBQ} = k_{ET}\eta_{\mathrm{DCBQ}} = 0$. Here, k_{ET} is the electron transfer rate, and η_{DCBQ} the concentration of DCBQ. We then measured a TA concentration series by the incremental addition of DCBQ to aliquots of wild-type cells from the same cell culture. These measurements were performed under identical conditions immediately after one another. We fix k_1, k_2 and k_3 from the wild-type cells without DCBQ, and then determine k_{DCBQ} as a function of DCBQ concentration from the samples with the addition of DCBQ.

Given our model, we can estimate the proportion of the CT states which decay through the DCBQ pathway through the quantum yield of DCBQ mediated electron transfer:

$$\phi_{ET} = \frac{k_{ET}\,\eta_{\mathrm{DCBQ}}}{k_2 + k_{ET}\eta_{\mathrm{DCBQ}}},$$

Equation 8

Based on our knowledge of $k_{ET}\,\eta_{\mathrm{DCBQ}}$ and the individually obtained rate constants for the cell (k_2), we can then determine the extraction for each specific concentration, $\phi_{1mM} = 17\%, \phi_{2mM} = 20\%, \phi_{4mM} = 25\%, \phi_{5mM} = 27\%$.

Equation 9

Uncertainty in the cell (without artificial quinone) lifetime is $\tau_{SE} = \frac{s}{\sqrt{n}} = 0.657$ ps, where s is the standard deviation and n is the number of biological replicates, in this case 5. The standard error in $k_{ET} = 2.4 \times 10^{-6}$mM^{-1}. We assume no error in the concentration of DCBQ. This gives the associated error in extraction efficiency as:

$$\delta\phi_{1mM} = 17\% \sqrt{\left(\frac{2.4 \times 10^{-6}}{8.5 \times 10^{-6}}\right)^2 + 2\left(\frac{0.657}{5.112}\right)^2} = \pm 5.7\%$$

Equation 10

1.5.4. DCBQ acts upon photosystems in living cells that are fully assembled and intact

DCBQ is reduced by the early CT state of fully assembled and intact photosystems where the P680 or P700 is embedded > 2 nm from the periphery of the protein scaffold. We have observed DCBQ to act on the early CT state of the photosystems both *in vitro* and *in vivo.* The isolated photosystem preparations are of high purity and homogeneity as dimers of PSII and trimers of PSI because during preparation we control for this through chromatography.[3,34,35]

However, the photosystems in cells are assembled in intermediate stages, some of these so-called 'assembly intermediates' could expose the P680 and P700 < 2 nm from DCBQ, and need to be considered.[36] We conclude that the TA would not be sensitive to assembly intermediates which have a different bleach to the intact photosystems. There is evidence from steady-state absorption measurements suggesting that Chl *a* pigments retain a differing bleach signal based on their protein scaffold environment.[37] However, in the worst case, assuming that both populations of photosystems (i.e. assembly intermediates and fully assembled photosystems) absorb identically, would suggest in wild-type cells that the TA signal is

comprised of a mixture of assembly intermediates and fully assembled photosystems. For example, if the assembly intermediates were 10% of the total population, this would suggest approximately -0.04 mΔOD of the signal may be attributed to assembly intermediates.

However, the addition of DCBQ affects the dynamics we observe significantly. Supposing again, in a worst-case scenario, where DCBQ only quenches disconnected chlorophylls and assembly intermediates, this suggests that 90% of the transient signal must remain unchanged, whereas 10% of the initial signal would decay over the timescale we have identified. This is not observed in the data.

Reviewing **SI Figure 13** – TA of wild-type *Synechocystis* cells in the presence of DCBQ and DMSO**,** the 710 nm feature is suppressed much further than would be expected if it were coming from a subpopulation of intermediates. The relative ratio of the 685 nm peak and the 710 nm feature, which in **SI Figure 13** – TA of wild-type *Synechocystis* cells in the presence of DCBQ and DMSO **D** is close to 1:2, where it is 1:1 with DCBQ addition (see green trace). This is a significant change, and >30% in terms of the kinetic model, but in terms of signal intensities, it is greater than a 50% signal reduction of the 715 nm peak relative to the 685 nm peak. This cannot be explained with impurities or assembly intermediates.

Further, photosystems in cells were found not to degrade significantly during TA measurements (**SI Figure 1** - Cell lifetime under laser illumination.), which might expose the internal cofactors, including P680 and P700, to DCBQ.

In any case, as the extraction efficiency for DCBQ is so great, specifically 17 ± 5 % at 1 mM DCBQ and as high as 27% for 5 mM DCBQ, even if DCBQ is reduced by subpopulations of photosystems in their assembly intermediate states, DCBQ must also be reduced by the main population of fully assembled photosystems.

1.5.5. DCBQ quenching mechanism

If the DCBQ-photosystems interaction that results in the observed ps time scale quenching phenomena relies on energy transfer, spectral overlap between the donor and acceptor has to exist. These may be resolved from absorption and photoluminescence measurements. From our measurements it becomes apparent that DCBQ does not have required accessible states, in particular spectral overlap for energy transfer. We therefore discount energy transfer in the DCBQ case. We note that Dexter energy transfer also only proceeds if the spectral overlap is non-zero, as encoded through the spectral overlap integral.

If the interaction is based on electron transfer, while it must be short ranged, it does not require spectral overlap, and it would scale with concentration. Our experimental results are consistent with these requirements. The mid-point potential of DCBQ (+0.315 V vs SHE at pH 7) makes it suitable to extract electrons from PSI also ($P700^*/P700^+$ = -1.290 V, F_B/F_B^- = -0.590 V) and PSII ($P680^*/P680^+$ = -0.660 V). Structural modelling (see below) suggests there exist sites where DCBQ may bind to peripheral chlorophyll pigments. Upon illumination and the formation of the delocalised charge, electron transfer from the peripheral chlorophyll to the mediator will be possible as understood from Marcus theory.

Among the other mechanisms, neither exciplex formation, collisional quenching or static quenching are sufficient to explain our results of an ultrafast accelerated decay in P680/P700. We have tabulated the various mechanisms in **Error! Reference source not found.**.

Table 2 Quenching mechanismsMechanism	Physical Description	Relevance to our System	References
Dynamic Quenching			
FRET	An RC, in its electronic excited state, may transfer energy to an acceptor through nonradiative dipole–dipole coupling.	No overlap between non-reduced DCBQ absorption and PL of RCs. No accessible states.	383940
Dexter	Bilateral exchange of electrons.	No overlap between non-reduced DCBQ absorption and PL of RCs. No accessible states.	41
Excimer Formation	Short molecule formed from two species, which would not bond if in ground state.	Exciplex formation should be a shallow state, with broad features, which we do not observe.	4243
Static Quenching			
Static Quenching	Ground state complex formed before excitation.	1- Would result in no change in excited state lifetime, contrary to our results 2 – Cell and DCBQ absorption spectrum do not change from cell spectrum.	44
Other Mechanisms			
DCBQ Induced Vibrational Relaxation	Changes in structure result in increased thermalisation rate to the ground state.	Invokes the generation of new phonons mediated by DCBQ, unlikely given structure of RCs.	
Diffusion	Excited RC encounters atom that facilitates non-radiative decays	Too slow to act on fs timescale when understood through kinetic theory.	45
Electron Transfer	Electron moves from electron donor to electron acceptor.	Short range and requires suitable energetics and binding sites, which we have identified.	4246

1.6. Addition of DCMU along with DCBQ (or other screened benzoquinones) to wild-type cells

To compare the effect of different benzoquinones we carried out TA experiments on wild-type *Synechocystis* cells, with and without different benzoquinones along with their associated solvents (DMSO, ethanol, SDS). DMBQ and PPBQ are benzoquinones that have been shown in previous studies to enhance photocurrent output from eukaryotic algae but not as efficiently as DCBQ,[47–50] which we confirmed in cyanobacteria (see **SI Section 4**). SDS is a detergent used to aid solubilisation of DMBQ and PPBQ in ethanol as they are otherwise insoluble in aqueous BG11 medium.

Neither 1 mM DMBQ or 1 mM PPBQ, or equivalent control experiments with only solvent added, demonstrated quenching (**SI Figure 15A -** compare τ_1, τ_2, τ_3 lifetimes of cells in green with cells + control quinones in blue). As already demonstrated in **Figure 1D-E**, DCBQ addition demonstrated a decrease in lifetimes compared to that of cells with no additives (**SI Figure 15A** - compare τ_3 lifetimes of cells in green with cells + 1 mM DCBQ in orange).

To compare the timing of action of DCBQ relative to the Q_B pocket in PSII we carried out TA experiments with DCBQ in conjunction with 3-(3,4-dichlorophenyl)-1,1-dimethylurea (DCMU). DCMU is known to bind to the Q_B pocket in PSII,[51] competing against benzoquinone docking there and reduction thereafter. We also tested DMBQ & DCMU and PPBQ & DCMU as controls. However, comparison of the raw lifetimes is more challenging here (**SI Figure 15B**), and needs further analysis. In the global fitting, each spectral component decays independently, so we cannot directly assign a specific component and hence a lifetime to quenching by DCBQ. Instead, each lifetime (τ_1, τ_2, τ_3) is weighted equally. The ratio of the lifetimes upon addition of DCBQ to that of wild-type cell sample with no benzoquinone addition is determined and plotted in **SI Figure 15C** (select samples also in **Figure 2d**). Samples which showed no difference in lifetimes would therefore have a mean ratio of 1. Only the difference in lifetimes after addition of DCBQ significantly deviated from 1 to approximately 0.5 (orange bar, first entry). Further, student t-tests comparisons between sample sets reveal that only the sample with DCBQ & DCMU (orange bar, fourth entry) had a meaningful change in lifetimes when compared to PPBQ, DMBQ, PPBQ & DCMU, and DMBQ & DCMU (all approximately 1). Therefore, upon the co-addition of DCMU, only the benzoquinone DCBQ demonstrated a statistically significant decrease in lifetimes ($p < 0.01$); this means we can determine that the action of DCBQ can be assigned to electron transfer steps before Q_B in the PETC.

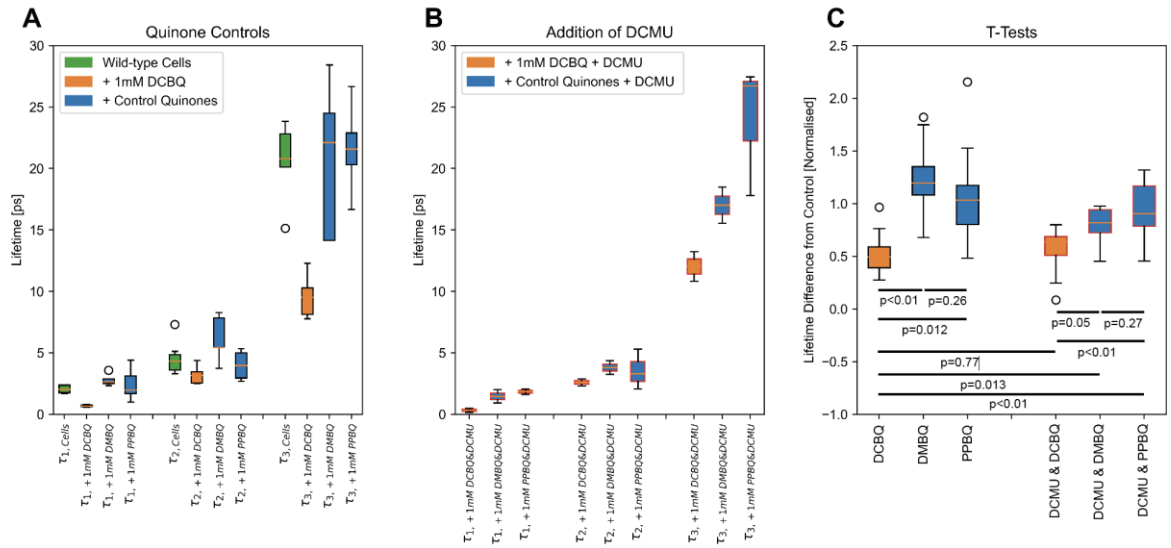

SI Figure 15 – Lifetimes with different benzoquinones and DCMU combinations.
A & **B)** Lifetimes. **A)** Benzoquinones DCBQ, PPBQ or DMBQ each 1 mM added to wild-type *Synechocystis* cells. Neither DMBQ or PPBQ (blue) show a measurable change the transients in the early timescale compared to cells with no additives (green) as DCBQ (orange) does. Data from three biological replicates. **B**) Benzoquinones DCBQ, PPBQ or DMBQ each 1 mM added to wild-type *Synechocystis* cells along with DCMU (1 mM). Data from two biological replicates. **C**) Ratio of lifetimes ($\tau_{WT}/\tau_{Additive}$) of cells with no additives, and cells treated with benzoquinones (panel A) and DCMU combinations (panel B).

1.7. Addition of DCBQ to the different biological samples

To determine the location of early time DCBQ mediated electron extraction within the cell, we carried out TA experiments with and without DCBQ on the different biological samples with varying photosystems

(described in **SI Section 1.2,** not including the Olive mutant). TA spectra of the different biological samples without DCBQ added is presented in **SI Figure 7**. Singular Value Decomposition of the TA spectra of the different biological samples with DCBQ added is presented in **SI Figure 10** and **SI Figure 11.** This section presents the TA data from experiments with DCBQ, and comparisons of that data with TA data from experiments without DCBQ.

Biological samples that contain functional PSI, which includes PSII-less cells (**SI Figure 16**) and isolated PSI (**SI Figure 17**), exhibited similar lifetimes for the long component. As described in **SI Section 1.4.2** (**SI Figure 10**), three components were retained in the PSII-less cells and two components for isolated PSI. The reduction in the lifetime of these components as a function of DCBQ concentration is more extreme in the isolated system (isolated PSI) compared to *in vivo* (PSII-less cells). PSII-less cells exhibited a reduction in τ_2 upon addition of DCBQ, whereas this is not observed in short lifetime component of isolated PSI.

Biological samples that contain functional PSII only, which includes PSI-less cells (**SI Figure 18**) and isolated PSII (**SI Figure 19**) show markedly different spectral features from those observed in the wild-type cells (previously described in **SI Section 1.2** (**SI Figure 7**). The long component (~ 1 ns) is two orders of magnitude greater than that observed in biological samples that contain functional PSI including wild-type cells (~ 30 ps). This long component does not meaningfully change upon the addition of DCBQ in biological samples that contain functional PSII. However, the shorter lifetime in biological samples that contain functional PSII exhibits a DCBQ mediated decay. The short lifetime decrease is otherwise difficult to deconvolute from the combined PSI and PSII signals in this region in wild-type cells. This is because the spectral features have significant overlap, as well as the lifetimes being similar in magnitude. PSI-less cells also have a smaller transient signal magnitude, likely arising from the fact that PSI has a 4-fold higher chlorophyll count compared to PSII. We were unable to increase the concentration of the cells in the TA experiments to get greater signal, as scattering overwhelmed the probe signal.

Although we have shown that electron extraction may occur from both PSI and PSII, both in cells and in isolation, is it difficult to determine with certainty the portion of charge extracted from PSI and, separately, from PSII in the wild-type cells. However, the similarity in the magnitude of lifetime reduction upon the addition of DCBQ, tends to suggest we are most sensitive to the CT state in PSI in the TA experiments described here.

Calculated lifetimes from all TA experiments are reported in **SI Tables 1-9**.

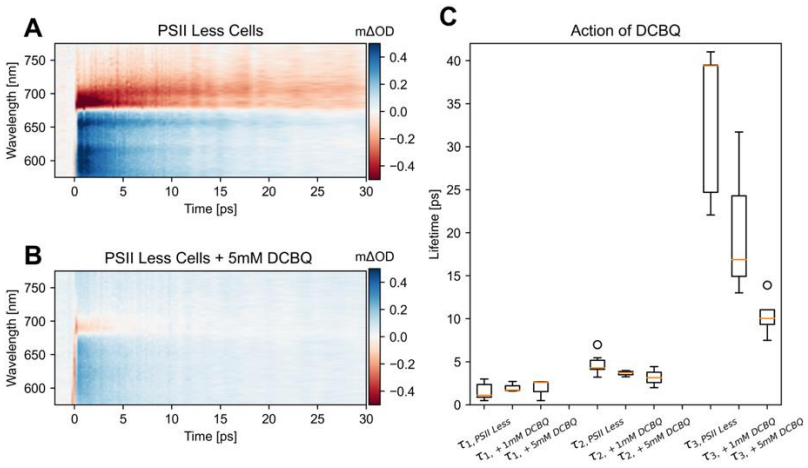

SI Figure 16 – Analysis of PSII-less cells in the presence of DCBQ
A) TA map of PSII-less cells before the addition of DCBQ. **B**) TA map of PSII-less cells with 5% DMSO and 5 mM DCBQ. Neither map is normalised, and both were measured under the same experimental configuration. **C**) As outlined in SI Figure 10, three components of the PSII-less mutants were retained and three associated lifetimes were determined from the global fit. The lifetimes closely match that of the wild-type cells. Data in panel C is from 3 to 5 biological replicates and maps in panels A and B are from one sample representative of replicates.

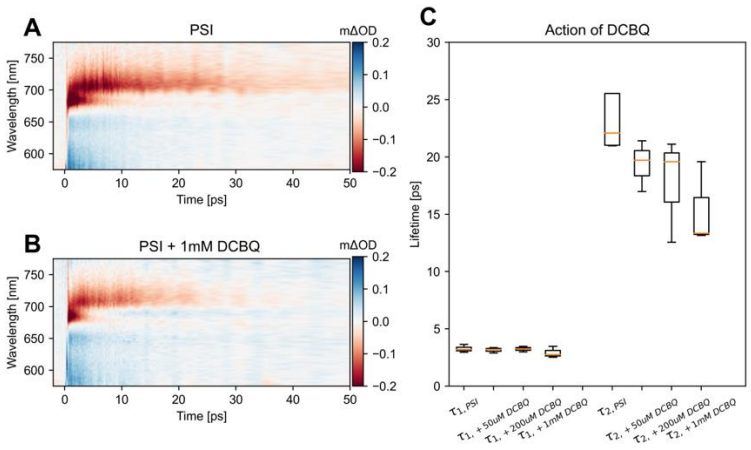

SI Figure 17 - Analysis of isolated PSI proteins in the presence of DCBQ.
A) TA map of isolated PSI before the addition of DCBQ. **B**) TA map of isolated PSI with 1% DMSO and 1 mM DCBQ. Neither map is normalised, and both were measured under the same experimental configuration. **C**) As outlined in SI Figure 10, two components from isolated PSI were retained and two associated lifetimes were determined from the global fit. The lifetimes closely match that of the wild-type cells. Data in panel C is from 3 to 5 biological replicates and maps in panels A and B are from one sample representative of replicates.

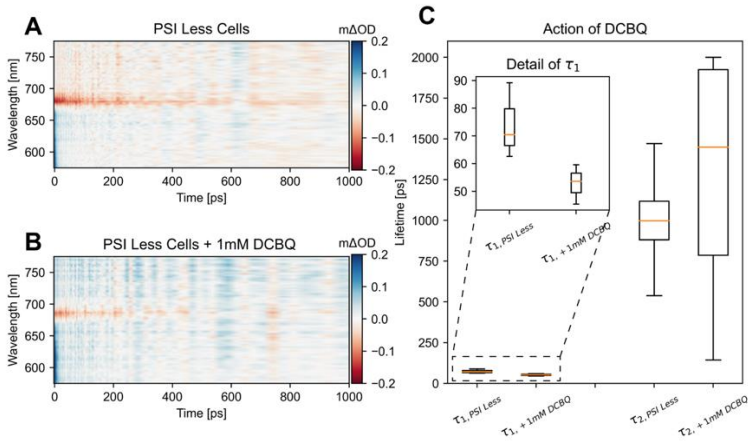

SI Figure 18 - Analysis of PSI-Less cells in the presence of DCBQ.
A) TA map of PSI-less cells before the addition of DCBQ. **B**) TA map of PSI-less cells with 1% DMSO and 1 mM DCBQ. Neither map is normalised, and both were measured under the same experimental configuration. **C**) As outlined in SI Figure 11, two components from PSI-less cells were retained, and two associated lifetimes were determined from the global fit. Data in panel C is from 3 to 5 biological replicates and maps in panels A and B are from one sample representative of replicates. The longer lifetime, on the order of 1 ns does not significantly change upon the addition of DCBQ, it is also difficult to compute with accuracy due to the reduction in signal from the sample with addition of DCBQ at long times. The shorter lifetime, plotted in detail in the inset, does show a reduction upon the addition of DCBQ.

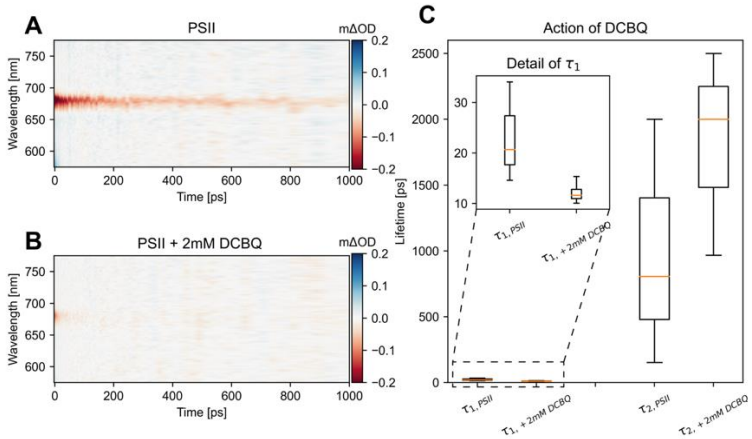

SI Figure 19 - Analysis of isolated PSII in the presence of DCBQ.
A) TA map of isolated PSII before the addition of DCBQ. **B**) TA map of isolated PSII with 2% DMSO and 2 mM DCBQ. Neither map is normalised, and both were measured under the same experimental configuration. **C**) As outlined in SI Figure 11, two components from of isolated PSII were retained, and two associated lifetimes were determined from the global fit. Data in panel C is from 3 to 5 biological replicates and maps in panels A and B are from one sample representative of replicates. The longer lifetime, on the order of 1 ns does not meaningfully change upon the addition of DCBQ and has significant uncertainty due to the reduction in signal from the DCBQ sample. The shorter lifetime, plotted in detail in the inset, does show a reduction upon the addition of DCBQ and is shorter than of the PSI-less cells.

1.8. Addition of methyl viologen to the PSI

Methyl viologen (MV^{2+}) is the most common electron mediator in artificial photosynthesis for electrocatalysis to facilitate chemical transformations (e.g. hydrogenases for hydrogen evolution). To demonstrate that higher-energy electrons can be extracted from photoexcited reaction centres by this class of mediators, TA experiments were performed on isolated PSI with and without MV^{2+} (–0.325 V vs SHE for the $MV^{2+}/MV^{+\bullet}$ redox couple at pH 7)[52].

The spectral components of isolated PSI exhibited diminished lifetimes in the presence of MV^{2+} (**SI Figure 20**), comparable to those seen in the presence of DCBQ. The extinction coefficient and population of the reduced species limit observable rise in the red to below the signal to noise limit of our system. Nevertheless, these results suggest MV^{2+} can also oxidise peripheral chlorophyll pigments of PSI.

We found that MV^{2+} had no effect when added to cell suspensions (cell results not shown here). MV^{2+} has been documented to be impermeable when oxidised and very weakly permeable when reduced in *E. coli* cells.[53,54] Furthermore, *in vivo* use of MV^{2+} as an electron mediator is limited by its high toxicity, which is attributed to its PSI oxidation and generation of reactive oxygen species. Trade-offs between the mid-point potential, photocurrent generation and toxicity of electron mediators has been explored in previous studies[55]. Future research can utilise TA to guide the design and synthesis of electron mediators with fast kinetics, favourable energetics, and low cytotoxicity.

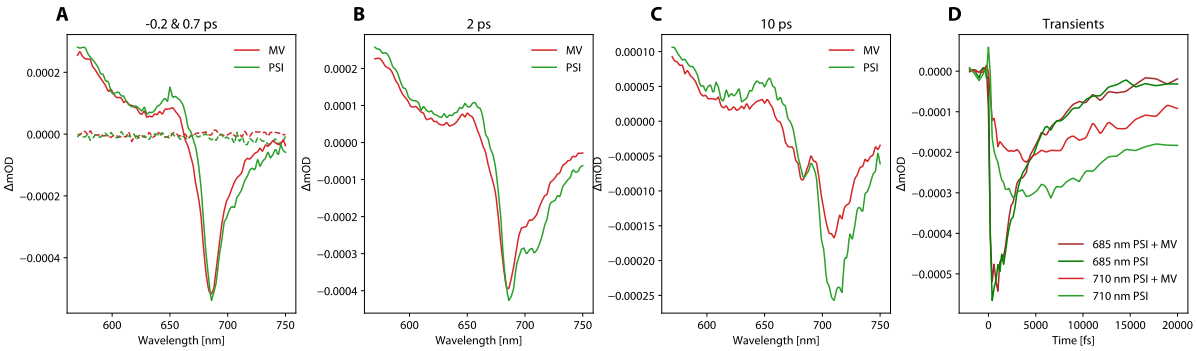

SI Figure 20 - Analysis of isolated PSI in the presence of MV^{2+}.
A) TA spectra of isolated PSI with and without MV^{2+}. Dashed line is at -0.2 ps. **B** & **C**) – TA spectra at 2 and 10 ps. **D**) TA transients at 685 nm and 710 nm, highlighting the supressed rise of the 710 nm feature and accelerated decay dynamics. MV^{2+} sample has been rescaled to match PSI bleach at 200 fs. Plotted data are of one sample, representative of 4 biological replicates.

2. UV-Visible Steady State Absorption and Spectroelectrochemistry

To determine whether DCBQ could participate in energy transfer mechanisms in the form of Dexter or Förster resonances from PSII *in vivo* or *in vitro*, the optical properties of separate solutions of the biological samples and DCBQ were characterised. The absorption spectrum of cells was dominated by broad scattering background, which was less present in isolated PSII (SI Figure 21)**.** Prominent absorption bands at 450, 680 and 700 nm correspond to the chlorophylls in the PSII and PSI complexes in cells. The absorption band at 622 nm corresponds to the phycobilisomes in cells. The absorption spectra of DCBQ in its neutral and reduced forms in BG11 medium and MES buffer displayed peaks at less than 300 nm (SI Figure 21)**.** The lack of overlap in the absorption spectra between DCBQ before reduction and the photosystems fluorescence *in vivo* indicates that energy transfer mechanisms, such as Förster resonances, could not be active in DCBQ-mediated quenching.[56] DCBQ must hence act with an electron transfer mechanism when extracting charge from photoexcited photosystems.

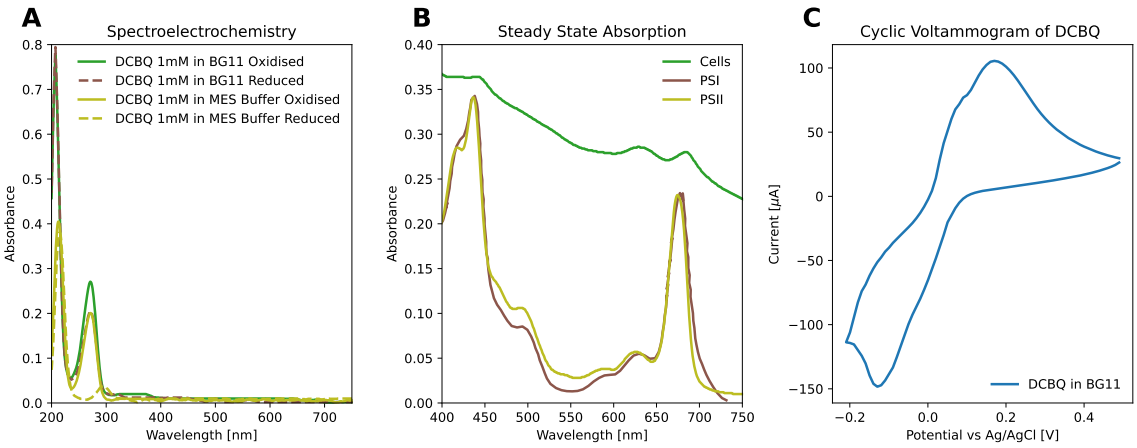

SI Figure 21 – Spectro-electrochemical characterisations of DCBQ and UV-vis absorption of biological samples.
A) DCBQ in neutral (without applied potential) and partially reduced (–0.1 V vs Ag/AgCl for 30 min, without stirring) forms in BG11 medium used for cells and MES buffer used for isolated photosystems. **B**) Biological samples wild-type *Synechocystis* cells and isolated photosystem I & II. **C**) Cyclic voltammogram of DCBQ (1 mM) in BG11 medium, under atmospheric conditions with applied potential 0.5 V to -0.2 V, 0.01 V steps, 0.05 V s-1 at pH 8.5 at 25°C.

To investigate if DCBQ was binding to the photosystems *in vivo* and *in vitro* and that it was changing its optical properties, the optical properties of solutions of the biological samples mixed with DCBQ were measured. Absorption spectra were measured 5 min after each addition. A final reading at the maximum concentration of DCBQ tested (5 mM) was repeated after an additional 20 min (exceeding the maximal length of a transient absorption spectroscopy run). The peaks in the absorption spectra for all cell and DCBQ solutions did not shift (**SI Figure 22**). We conclude that DCBQ is not tightly binding to the reaction centre chlorophylls. Controls DMSO solvent (0.2 – 5 %) and DCMU (1 mM) were also tested and found not shift the absorption spectra.

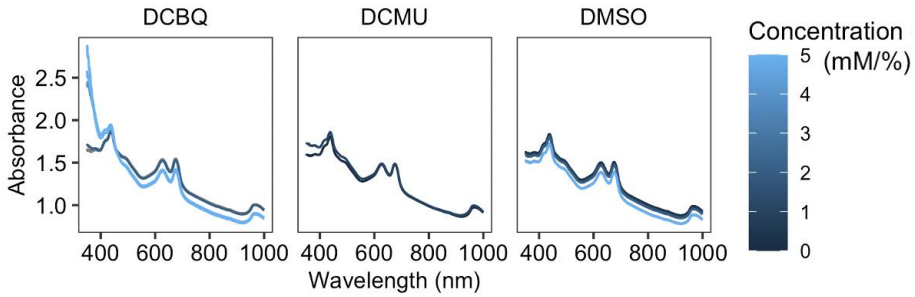

SI Figure 22 - Absorption spectra of *Synechocystis* cells mixed with spectroscopy additives.
Wild-type *Synechocystis* cells were mixed with 0.2 – 5 mM DCBQ (in 0.2-5% DMSO), 1 mM DCMU (in 1% DMSO) or 0.2-5% DMSO. Concentration in the key in mM for DCBQ and DCMU or % for DMSO. Absorption spectra was measured 5 min after each addition. A final reading at the maximum concentration of DCBQ tested (5 mM) was repeated after an additional 20 min (approximate length of a transient absorption spectroscopy run).

3. Structural studies

3.1. Location of primary electron donors within the photosystem protein complexes

Marcus theory describes how electrons may tunnel between cofactors when they are separated by approximately 2 nm (20 Å) or less.[57] Therefore, for electron transfer to occur from the early photoexcited state of photosynthetic reaction centres to DCBQ, the primary electron donors (P680/P700) and DCBQ would need to be within 2 nm of each other. Using PyMOL, we measured the distances between the primary electron donors and the edge of the protein scaffold of the photosystem protein complexes. The distance between the primary electron donors and any known binding pockets/docking sites within the protein scaffold were also determined.

PSII exists as a dimer in oxygenic photosynthetic organisms, although monomers have also been isolated from cells.[58] The structure of a PSII dimer from *T. elongatus* under room temperature, two-flash illumination and 'damage-free' conditions (using an X-ray free electron laser) at 2.25 Å resolution by Young *et al*. (2016) (Protein Data Bank ID: 5TIS) was analysed.[59] In each monomer in the PSII dimer, the primary electron donor associated with the D_1 (PsbA) protein subunit (P_{D1}, one of the chlorophyll molecules in the P680) was measured to be ~40 Å from the cytoplasmic side of the protein scaffold and 24.1 Å from Q_B in the Q_B binding pocket (**SI Figure 23A**), both greater than 2 nm for fast electron transfer to occur.

In most cyanobacteria, PSI exists as a trimer under optimal conditions although is also present as a monomer as a small fraction of the total amount of PSI.[60] Under different growth conditions, such as iron limitations or high temperatures the ratio of monomers to trimers shifts toward the monomeric form.[61,62] It is generally accepted that in plants and algae PSI is monomeric.[63–66] The X-ray crystal structure of a PSI monomer from the cyanobacterium *Synechococcus elongatus* at 2.5 Å resolution by Jordan *et al*. (2001) (Protein Data Bank ID: 1JB0) was analysed.[67,68] While in PSI there is no established intraprotein binding pocket like the Q_B binding pocket in PSII, there are putative docking sites for ferredoxin (Fd) (or flavodoxin under iron limitation) at the cytoplasmic side (or stromal side in eukaryotic oxygenic photosynthetic organisms) and for plastocyanin (Pc) (or Cyt c_6 under copper limitation) at the luminal side.

While the exact locations of these docking sites have not been established, the docking site for Fd is hypothesised to be in a pocket formed by protein subunits PsaC, PsaD and PsaE,[67] the location of which for distance measurements was approximated as the central C atom of the aspartic acid residue at position 66 in the PsaC protein subunit. In the PSI monomer, the primary electron donor associated with the PsaA protein subunit in the A-branch (P_A, one of the chlorophyll molecules in the P700) were measured to be 48.7 Å from the putative Fd docking site (also the cytoplasmic side of the protein scaffold) (**SI Figure 23B**).

The docking site for Pc is hypothesised to be a hollow close to the pseudo-C_2 axis formed by α-helices of the PsaA and PsaB protein subunits.[67,69] Tryptophan residues from PsaA and PsaB protrude into the hollow and are hypothesised to engaged in interaction with and/or electron transfer from Pc to the oxidized primary electron donor $P700^{+\bullet}$.[67,69] The location of the putative Pc docking site was approximated for distance measurements as the C_4 atom of the indole group of the tryptophan residue at position 631 in the PsaB protein subunit. P_A was measured to be 11.4 Å from the putative Pc-docking site, which was less than the 2 nm maximum for electron transfer to be permissible under the limits imposed by Marcus theory.

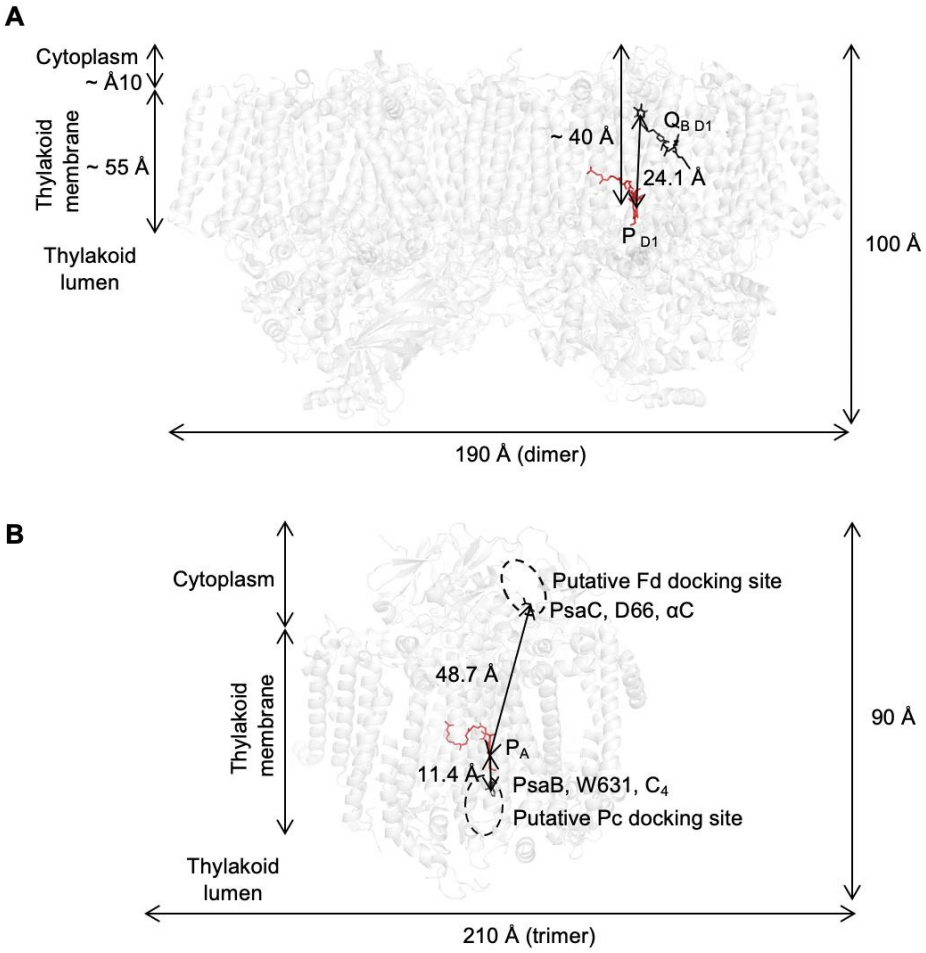

SI Figure 23 - Location of the primary electron donors within the photosystem protein complexes.
A) Structure of the photosystem II (PSII) dimer (grey transparent ribbons) showing the locations and distances between the primary electron donor (P_{D1}, red) and the terminal quinone ($Q_{B\ D1}$, black) in the Q_B pocket and the edges of the protein scaffold. Ring-to-ring distance between P_{D1} and $Q_{B\ D1}$ 24.1 Å, distance between P_{D1} and the cytoplasmic side of the protein scaffold ~40 Å, both greater than 2 nm for electron transfer, calculated using PyMOL. Structure rendered in PyMOL from the crystal structure by Young et al. (2016) (Protein Data Bank ID: 5TIS).[59] **B)** Structure of the photosystem I (PSI) monomer (grey transparent ribbons) showing the locations and distances between the primary electron donor (P_A, red) and the putative ferredoxin (Fd) and pyocyanin (Pc) docking sites (dashes ovals), amino acids in the putative doxing sites as a proxy for their location (black) and the edges of the protein scaffold. Distance between P_A and the central C atom of the aspartic acid residue at position 66 in the PsaC protein subunit (PsaC, D66, αC) 48.7 Å, greater than 2 nm for electron transfer. Distance between P_A and the C_4 atom of the indole group of the tryptophan residue at position 631 in the PsaB protein subunit (PsaB, W631, C_4) 11.4 Å, less than 2 nm for electron transfer. Distances calculated using PyMOL. Structure rendered in PyMOL from the crystal structure by Jordan et al. (2001) (Protein Data Bank ID: 1JB0).[67]

3.2. Location of chlorophylls within the photosystem protein complexes

However, all chlorophylls embedded within the reaction centres are energetically degenerate at room temperature.[70,71] Photoexcitation thus results in a highly delocalised excited state shared across several chlorophylls (described by the Lake Model of photoexcitation).[70,71] At the sub-picosecond timescale, the reaction centres are in a delocalised charge-transfer state capable of charge transfer.[72,73] Indeed, there are

chlorophylls less than 2 nm inside from the edge of the protein scaffold, including four that protrude from the PSII dimer (**SI Figure 24A**, in yellow) and 14 that protrude from the PSI monomer on sides not against anther PSI monomer in the trimer (**SI Figure 24B**, in yellow)**.** Most of these protruding chlorophylls are in the sections of the photosystem protein complexes within the thylakoid membrane. Only the top ~10 Å of PSII is exposed in the cytoplasm of cyanobacterial cells (or stroma of chloroplasts in plants and algae) and ~55 Å of PSII is located within the thylakoid membrane,[74] and so only the PsaC, PsaD and PsaE subunits of PSI are not in the thylakoid membrane. Notably, DCBQ is soluble in phospholipid bilayers so it may access to structures within in the thylakoid membrane, including the peripheral chlorophylls in the photosystems.

We conclude that upon photoexcitation of the photosynthetic reaction centres, the charge-transfer (CT) state extends to periphery chlorophylls within < 200 fs. Favoured at high concentrations, DCBQ was reduced by a periphery chlorophyll into the semiquinone radical (DCSQ•–), with potentially a second electron transfer to the fully reduced form (example for PSII and PSI illustrated in **Figure 2A** in the main text).

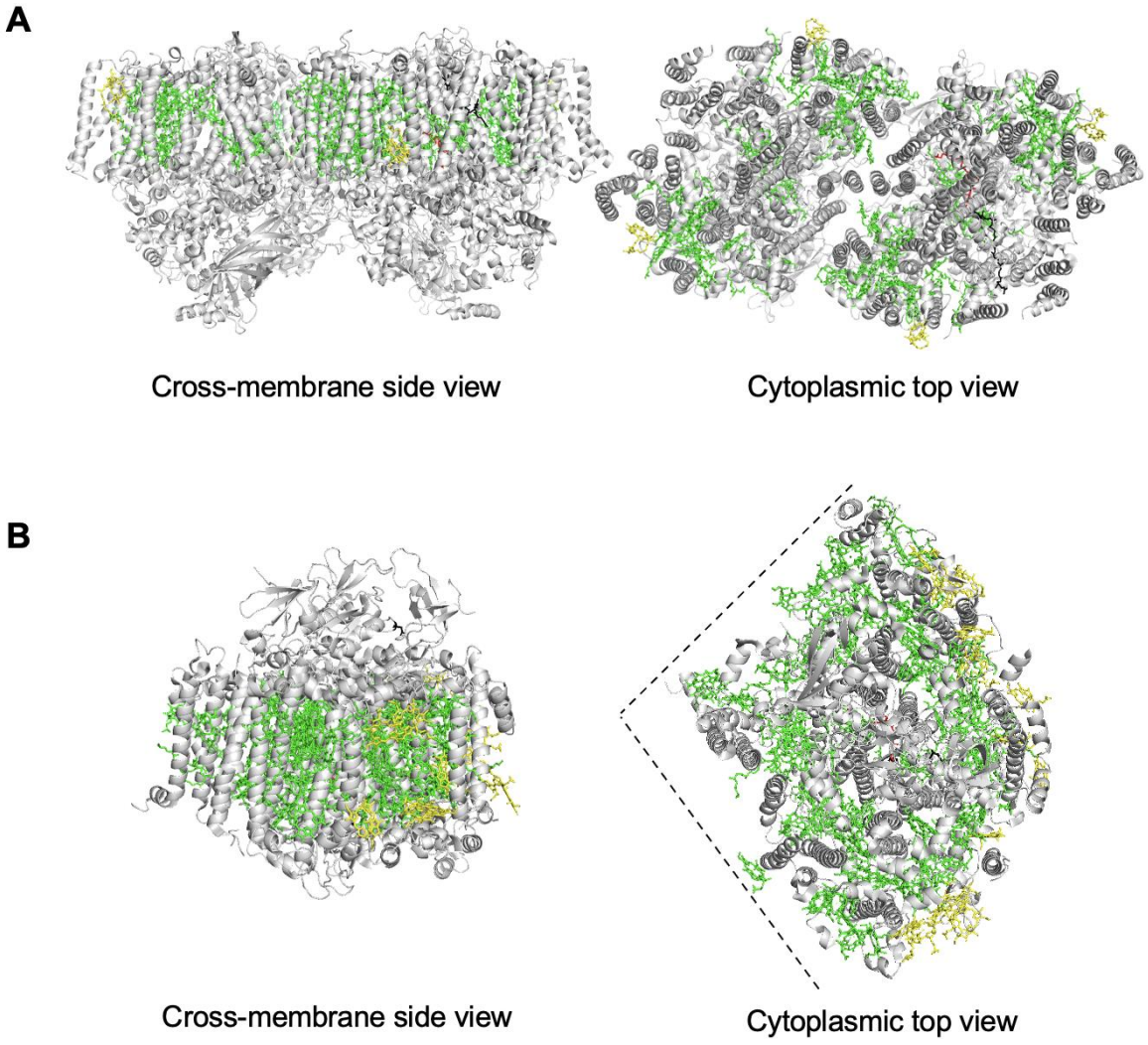

SI Figure 24 - Location of chlorophylls in the photosystem protein complexes
A) Structure of the photosystem II (PSII) dimer (grey ribbons), primary electron donor (P_{D1}, red), the terminal quinone ($Q_{B\,D1}$, black) in the Q_B pocket, chlorophylls (green), and some chlorophylls that protrude from the protein scaffold (yellow) that would enable DCBQ to associate at a distance less than 2 nm for electron transfer. Structure rendered in PyMOL from the crystal structure by Young et al. (2016) (Protein Data Bank ID: 5TIS).[59] **B)** Structure of the photosystem I monomer (grey ribbons), primary electron donor (P_A, red), amino acids in the putative Fd and Pc doxing sites as a proxy for their location (black), chlorophylls (green), and some chlorophylls that protrude from the protein scaffold (yellow) that would enable DCBQ to associate at a distance less than 2 nm for electron transfer. Dashed line indicates the sides of the monomer that link to other monomers in the trimer. Structure rendered in PyMOL from the crystal structure by Jordan et al. (2001) (Protein Data Bank ID: 1JB0).[67]

4. Photoelectrochemistry

The ability of a candidate benzoquinone molecule to enhance photocurrents stemming from *Synechocystis* cells and isolated PSII complexes was determined using photoelectrochemistry. In these experiments, the biological components were immobilised onto IO-ITO working electrodes of appropriate dimensions and

the photocurrent profiles were measured using chronoamperometry under light/dark cycles without and then with benzoquinones (and DCMU). Chronoamperometry was performed at an applied potential of 0.5 V vs SHE for maximal mediation by benzoquinones (as derived from previous stepped chronoamperometry and based on their mid-point potentials).[9,47,75] The photocurrent was measured as the difference between the steady-state current outputs in the light and dark periods. Photocurrent magnitudes with benzoquinone and DCMU were calculated relative to the neat sample with zero benzoquinone or DCMU as 1 arbitrary unit (a. u.). The extent of increased photocurrent output in the presence of the benzoquinone relative to the photocurrent output without the exogenous mediators indicate the ability of the benzoquinone to serve as a mediator between the PETC and the electrode.[76]

First, different benzoquinones were screened: DCBQ, phenyl-1,4-quinone (PPBQ) and 2,6-dimethyl-1,4-benzoquinone (DMBQ). Based on the concentration of benzoquinone tested in previous studies, 1 mM was chosen as the concentration of the different benzoquinones to test.[9] DCBQ (1 mM) increased the photocurrent of *Synechocystis* cells on IO-ITO electrodes approximately 50-fold (**SI Figure 25**). PPBQ (1 mM) and DMBQ (1 mM) each mediated less efficiently than DCBQ (1 mM), giving approximately 40-fold and 10-fold increases in photocurrent, respectively.

The effects of PPBQ and DMBQ on cells were greater with SDS detergent (8.2 mM final concentration), added to aid their solubilisation (**SI Figure 27**). This suggested that different solubility of benzoquinones in the aqueous BG11 medium (and also the aqueous cytosol of the cell) may account for differences in their ability to mediate. Indeed, it has been suggested before that benzoquinones can be sequestered in intracellular membranes and precipitate in aqueous compartments of the cell.[48] Nevertheless, there was some mediation without SDS with PPBQ and DMBQ (10% EtOH) giving approximately 20-fold and 5-fold increase in photocurrent, respectively, so the ultrafast transient absorption spectroscopy studies were able to be performed without SDS.

For isolated PSII on IO-ITO electrodes, DCBQ and PPBQ mediated similarly efficiently, increasing the photocurrent approximately 2-fold (**SI Figure 26**). This was consistent with the limited ability of PPBQ to efficiently mediate electrons *in vivo* being caused by its reduced ability to access PSII from the cytoplasm.

To determine the relationship between concentration of DCBQ and electron mediation efficiency, different concentrations of DCBQ were tested. For cells, the minimum concentration tested was 200 µM, which was the maximum concentration of DCBQ that was not cytotoxic to the cells over 12 h (**SI Figure 31**),[75] and the maximum concentration tested was 5 mM, which was the concentration that yielded a clearly observable difference in the transient absorption spectra. This concentration range included 1 mM, which was the concentration of benzoquinone tested in previous studies.[9] A minimum concentration of 50 µM was tested for isolated PSII. The maximal increase in photocurrent of *Synechocystis* cells on DCBQ treatment was approximately 50-fold at a concentration of 1 mM, and the increase dropped to 20-fold at 5 mM DCBQ (**SI Figure 26**). As with whole cells, the maximum mediation of photocurrent from isolated PSII was not seen at the highest concentration of DCBQ tested. The maximal increase in photocurrent of isolated PSII on DCBQ treatment was approximately 8-fold at a concentration of 200 µM, and only 2-fold at 1 mM DCBQ (**SI Figure 26**).

The fact that addition of DCBQ resulted in a bigger increase in photocurrent output for cells (50-fold) than for isolated PSII (8-fold) indicates that the isolated PSII were inherently more efficiently wired to the electrodes than whole cells, due to their participation in direct electron transfer to IO-ITO electrodes,[77] whereas cells participate in indirect electron transfer via an endogenous electron mediator.[9,78,79]

The effect of solvents used in the above experiments was tested. The increase of photocurrent output by exogenous benzoquinones was not due to the solvents/detergents in which they were dissolved. In fact, the solvents/detergents reduced the photocurrent output slightly (**SI Figure 27B**). However, none of the photocurrents of samples with solvents was statistically different from those without solvent.

To examine benzoquinone electron mediation upstream and downstream of Q_B, DCMU was tested in combination with the benzoquinones. First, the effect of the order of addition of the benzoquinone and DCMU to the cells or isolated PSII was tested with DCBQ (**SI Figure 25**). The order affected the photocurrent magnitude but not the trend: DCBQ and DCMU yielded higher photocurrents than DCMU only. Cells with DCBQ added before DCMU gave higher photocurrent than cells with DCMU added first, which was most likely due to cell death from the herbicide action. Isolated PSII with DCMU added before also adding DCBQ gave higher photocurrent than DCBQ added first, which was some evidence that the Q_B binding pocket was not the only site of mediation in PSII by DCBQ. For subsequent experiments DCMU was added after any benzoquinones.

It has been demonstrated that Q_A can participate in direct electron transfer from isolated PSII to the electrode as there is photocurrent from isolated PSII treated with DCMU but with no natural or exogenous electron mediators present.[80] Conversely, *Synechocystis* cells treated with DCMU yield no photocurrent. Therefore, Q_A cannot transfer electrons to the electrode when inside of cells.

It has also been demonstrated that small cationic molecules can interact with PSII near Q_A to extract electrons; with DCBQ being a poor molecular acceptor for sites near Q_A.[81,82] The photocurrent from *Synechocystis* cells in the presence of equimolar concentrations of DCBQ and DCMU was approximately one third of that without the herbicide present (**SI Figure 26**). The one third is what DCBQ mediates from PSII before Q_A, some of which we measured using TA; the missing two thirds must be mediation by DCBQ from Q_B and further downstream in the PETC, including from early in PSI. PPBQ and DMBQ did not mediate at all in the presence of DCMU. For isolated PSII, again, approximately one-third of photocurrent was yielded in the presence of equimolar DCMU and DCBQ, and PPBQ performed similarly to DCBQ (**SI Figure 26**). This is consistent with the cell membrane being a barrier for both PPBQ and DMBQ as mediators. Therefore, DCBQ was the only benzoquinone electron mediator screened that appeared to extract electrons at a point that is earlier than Q_B in PSII *in vivo*, which is consistent with the TA results.

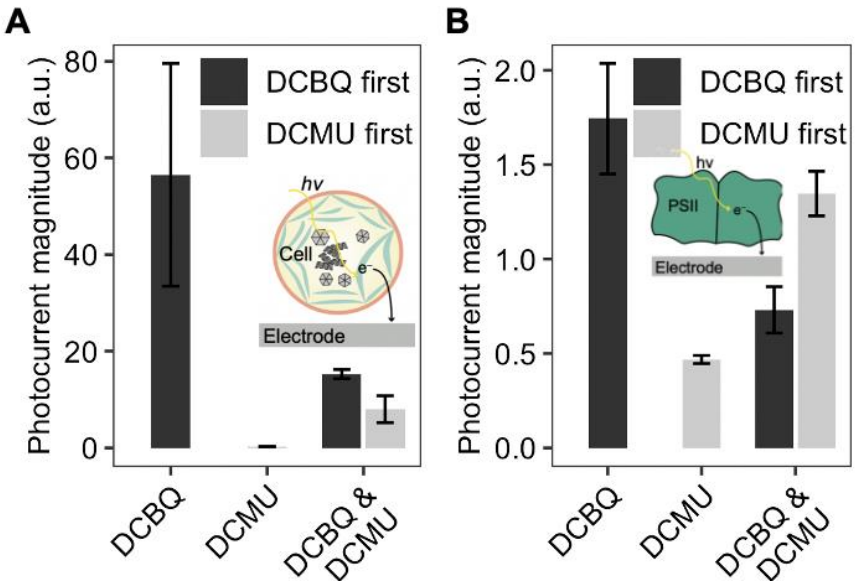

SI Figure 25 - Effect of the order of addition of DCBQ and DCMU on photocurrent enhancement by exogenous electron mediators.

A) *Synechocystis* cells, and **B)** isolated PSII. Photocurrent outputs with DCBQ (1 mM) and DCMU (1 mM) added in different orders. Photocurrent magnitudes calculated from the difference in steady state current density in the light and the dark. Photocurrent magnitudes with benzoquinone and DCMU were calculated relative to the neat sample with zero benzoquinone or DCMU as 1 arbitrary unit (a. u.). Photoelectrochemistry parameters include: 0.5 V vs SHE and a Ag/AgCl reference electrode and a Pt-mesh electrode, 25˚C, atmospheric conditions, BG11 medium (pH 8.5) electrolyte for cells and MES buffer (pH 6.5) electrolyte for PSII, 60 s/90 s light/dark cycles for cells and 15 s/15 s light/dark cycles for PSII, 50 $\mu mol_{photons}$ m^{-2} s^{-1} 680 nm light. Data presented as the average of three biological replicates ± standard error of the mean.

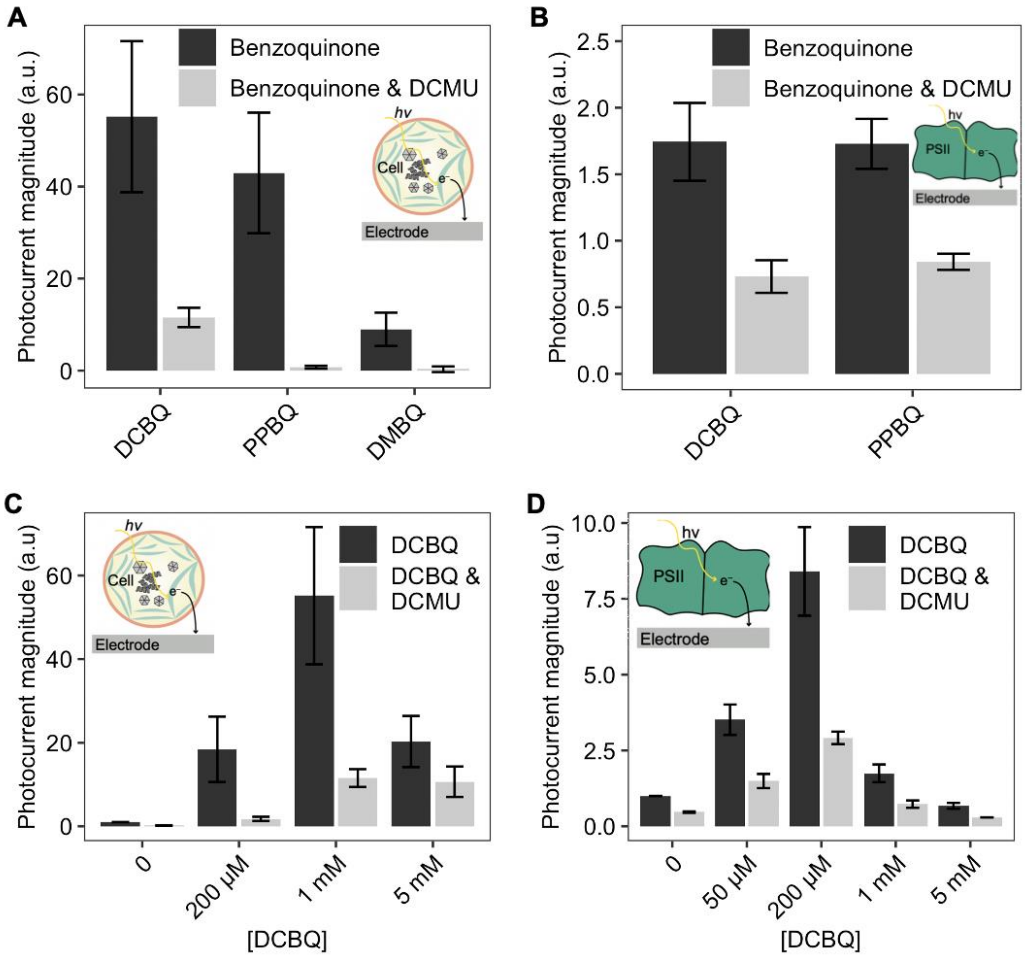

SI Figure 26 - Photocurrent enhancements from exogenous addition of benzoquinones
A) & C) *Synechocystis* cells, and **B) & D)** isolated PSII. **A) & B)** Photocurrent outputs with different benzoquinones (1 mM) added: 2,6-dichloro-1,4-benzoquinone (DCBQ), phenyl-1,4-quinone (PPBQ) and 2,6-dimethyl-1,4-benzoquinone (DMBQ). In the absence and presence of DCMU (1 mM). **C) & D)** Photocurrent outputs with different concentrations of DCBQ and DCMU (1 mM) added. Photocurrent magnitudes calculated from the difference in steady state current density in the light and the dark. Photocurrent magnitudes with benzoquinone and DCMU were calculated relative to the neat sample with zero benzoquinone or DCMU as 1 arbitrary unit (a. u.). Photoelectrochemistry parameters as in SI Figure 25. Data presented as the average of three biological replicates ± standard error of the mean.

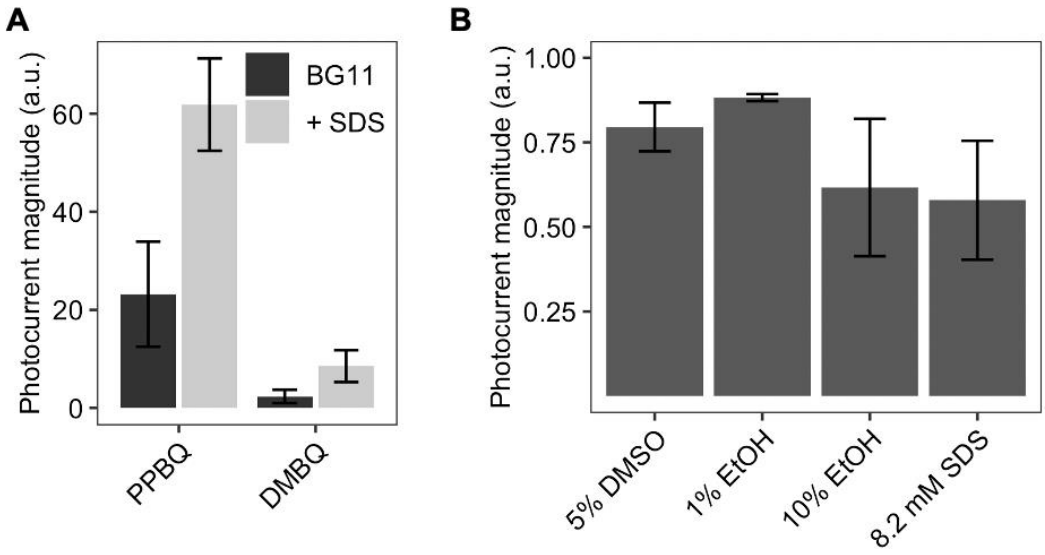

SI Figure 27 - Change in photocurrent of Synechocystis cells in the presence of solvents
A) Photocurrent outputs with PPBQ and DMBQ with and without SDS to aid solubilisation in aqueous BG11 medium used as the electrolyte. **B)** Change in photocurrent of Synechocystis cells in the presence of solvents. Photocurrent magnitudes calculated from the difference in steady state current density in the light and the dark. Photocurrent magnitudes with solvents were calculated relative to the neat sample in BG11 with zero solvent as 1 arbitrary unit (a. u.). Photoelectrochemistry parameters as in SI Figure 25. Data presented as the average of three biological replicates ± standard error of the mean. For panel B, raw photocurrent outputs were statistically non-significant.

5. Time-Correlated Single-Photon Counting Measurements

Previously, PSII has been studied *in vivo* in photosynthetic microorganisms via nano-second time-correlated single-photon counting (TCSPC).[83–86] To record the time-resolved photoluminescence decay of the samples, TCSPC was performed on isolated PSII and wild-type *Synechocystis* cells with DCBQ. The PSII reaction centres can be considered to be in an open or closed state. An open reaction centre has the primary quinone Q_A oxidized and ready to undergo stable charge separation, whereas a closed reaction centre has Q_A reduced to Q_A^-. In a closed reaction centre charge separation will be followed by fast charge recombination and enhanced chlorophyll fluorescence yield owing to the larger probability of decay via the chlorophyll excited state.[1]

Both PSII and PSII with DCMU (1 mM) displayed the long-lived chlorophyll emission indicative of closed reaction centres (**SI Figure 28-A,C**). PSII with DCBQ (1 mM) displayed a much shorter-lived emission, which is indicative of open reaction centres. The cells had much longer-lived emissions than the isolated PSII, and displayed the same effects of DCMU and DCBQ (**SI Figure 28-B,D**). Upon increasing the concentration of DCBQ, we observed a linear reduction in both lifetimes with concentration, reaching 1.2 ns $\pm$ 0.4 ns at the highest concentration of DCBQ tested in TCSPC (1 mM) for isolated PSII and cells, respectively. DMSO solvent did not measurably change the photoluminescence decays of cells (**SI Figure 29A-B**). BG11 medium controls assured us that the sample was the only emitting species at the pump wavelength (**SI Figure 29C**). These results indicated that DCBQ acted on PSII *in vivo* and *in vitro* within nanoseconds after photoexcitation.

Calculated lifetimes from TCSPC are reported in **SI Tables 10-12**.

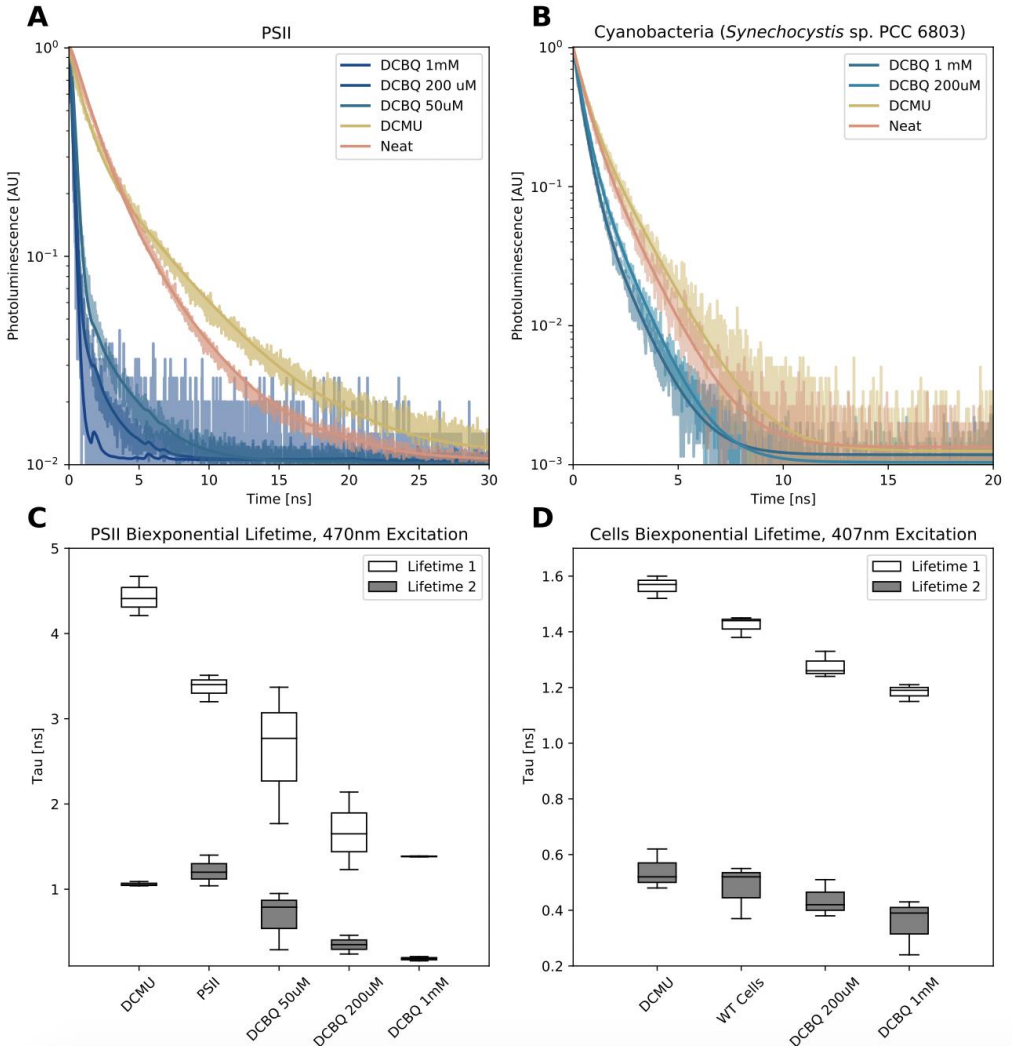

SI Figure 28 - TCSPC analysis of biological samples treated with DCBQ or DCMU.
A & **C)** isolated PSII treated with DCBQ or DCMU. **B** & **D)** Wild-type *Synechocystis* cells treated with DCBQ or DCMU. **A-B**) Time-resolved radiative decay dynamics. Wild-type cells exhibit radiative decay dynamics well described by a bi-exponential decay (solid line). **C-D)** Lifetimes.

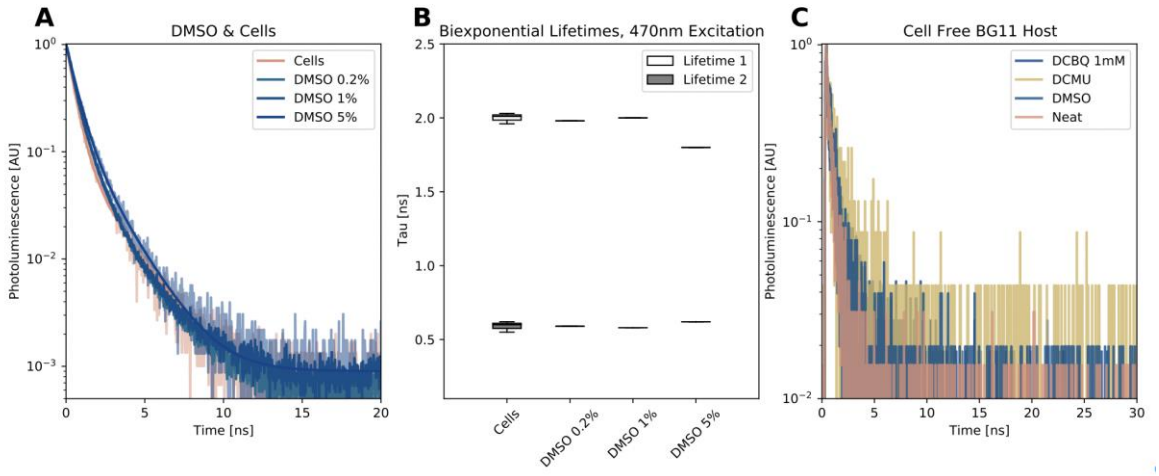

SI Figure 29 - TCSPC controls.
A & **C)** Time-resolved radiative decay dynamics. Wild type cells exhibit radiative decay dynamics well described by a bi-exponential decay (solid line) in panel A. **B)** Lifetimes of panel A. **A-B)** Wild-type *Synechocystis* cells treated with different volumes of DMSO solvent. **C)** BG11 medium with no cells with DCBQ, DCMU or DMSO added.

6. Oxygen Evolution

To confirm that PSII was performing photolysis of water *in vivo* in the presence of the difference concentrations of DCBQ, we measured oxygen evolution. Cells without DCBQ treatment showed healthy PSII activity for cells in early stationary phase of 23 ± 4 $\mu mol_{(O2)}\ mg^{-1}{}_{(Chl\ a)}\ h^{-1}$. In parallel, the cells were treated with different concentrations of DCBQ for 15 min prior to measuring oxygen evolution. The oxygen evolution of cells treated with DCBQ was normalised to that without DCBQ as 1 arbitrary unit (a.u.) (**SI Figure 30**). Cells treated with lower concentrations of DCBQ (≤ 1 mM) showed approximately half the PSII activity of untreated cells. Cells treated with higher concentrations of DCBQ (up to 5 mM) showed similar PSII activity to that of untreated cells, although with high variability between biological replicates. These results confirmed that PSII was performing photolysis of water *in vivo* in the presence of DCBQ even up to the highest concentrations and exposure times tested in the TA. The cause of the reduction of PSII activity *in vivo* after DCBQ treatment is the scope of future studies, although we did follow up with cytotoxicity assays that showed that high concentration DCBQ exposure for hours kills the cells (see **Section 7**). Further, even though cells were found to generate approximately half the number of electrons from water lysis in the presence of 1 mM DCBQ, they yielded 50-fold higher extracellular electron transfer to an electrode under illumination than untreated cells (see **SI Section 4**). This indicated that the dominant action of DCBQ is to compete with the downstream natural electron transfer pathways rather than increasing water oxidation rates by PSII.

Note that oxygen evolution was measured on the time scale of seconds after illumination like the photoeletrochemistry experiments, whereas the TA measurements probed events on the sub-picosecond timescale after photoexcitation. Oxygen evolution occurs by the Mn_4Ca cluster in PSII's oxygen evolving complex (OEC) completing the photo-induced Kok cycle, the final step of which takes 1 ms.[87] This is also the 4th step within PSII after photo-excitation of the P680, with the hole that formed by the 1st step (formation of the initial charge separated state with the primary electron acceptor pheophytin (Ph) [$P680^{+\bullet}$–Ph^{-}] that has a lifetime of 10-30 ps) migrating to the OEC to be filled by the electrons produced by

photolysis of water. Therefore, the OEC is the kinetic bottleneck during the re-wiring of electron transfer from the reaction centre in the presence of DCBQ.

The electrons produced from water oxidation by the OEC are shuttled via the electron transport chain to PSI through the plastoquinone (PQ) pool to the cytochrome b_6f complex (Cyt b_6f) and then through a plastocyanin (Pc) pool.[88] The bottleneck in re-wiring electron transfer from the P700 early after photoexcitation is diffusion of plastoquinone from the Q_B pocket in PSII to the cytochrome b_6f complex which takes approximately 10 ms.[88] However, before photoexcitation, the Pc pool is somewhat reduced[89] and is a short-term source of electrons for PSI before it is refilled by PSII action. This may account for why we found that the sub-picosecond reduction of DCBQ was dominated by PSI.

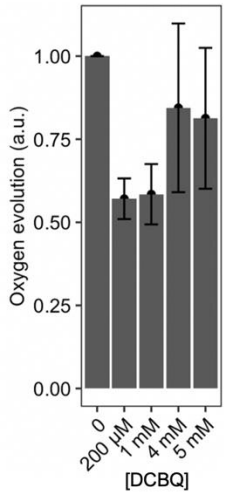

SI Figure 30 - Oxygen evolution of wild-type *Synechocystis* cells with DCBQ.
Measurement using 1500 $\mu mol_{photons}$ m^{-2} s^{-1} light at 627 nm. The electrolyte was BG11 medium (pH 8.5). Data presented as the mean of five biological replicates, error bars are standard error of the mean.

7. Cytotoxicity

In addition to assessing the health of the cells following laser irradiation experimental conditions (**SI Figure 1**), we also explored the longer-term effects of the benzoquinones on cells growth. Spot assays were performed. Equivalent amounts of wild-type *Synechocystis* cells to those that adhered to the IO-ITO electrodes after photoelectrochemical experiments (5 nmol Chl *a*) were incubated with concentration ranges of up to 5 mM for DCBQ, PPBQ and DMBQ for 1 day under constant light (50 $\mu mol_{photons}$ m^{-2} s^{-1} white light used for culturing). Three control conditions were also assayed: cells in BG11 (no mediator), and cells in BG11 with 5% (v/v) DMSO (the highest concentration of DMSO solvent for benzoquinone addition). After exposure to the mediators, the *Synechocystis* cells were re-suspended in fresh BG11 medium, spotted onto BG11 agar plates, and incubated for 1 week. The highest concentration of exogenous mediator at which the cells could still grow after 24 h exposure was identified (**SI Figure 31**). These results suggest that cytotoxicity artefacts are not the cause of the effect on the early CT state as PPBQ is more cytotoxic than DCBQ, however, only DCBQ showed a significant change on the early picosecond timescale.

Exogenously added DCBQ and DMBQ were non-toxic at concentrations ≤ 200 µM. However, even 200 µM PPBQ was toxic to the cells, with no growth observed. These results indicated that DCBQ (200 µM) was not

cytotoxic when the sub-picosecond after photoexcitation was measured to a small degree (**Figure 2C**). There was not a correlation between the cytotoxicity of the different benzoquinones or the concentration of DCBQ that killed cells (**SI Figure 31**) and their ability to re-direct electrons from the electron transport chain and enhance extracellular electron transfer to an electrode (see **SI Section 4**). There was also not a correlation between the concentration of DCBQ that killed cells (**SI Figure 31**) and the PSII activity (**SI Figure 30**).

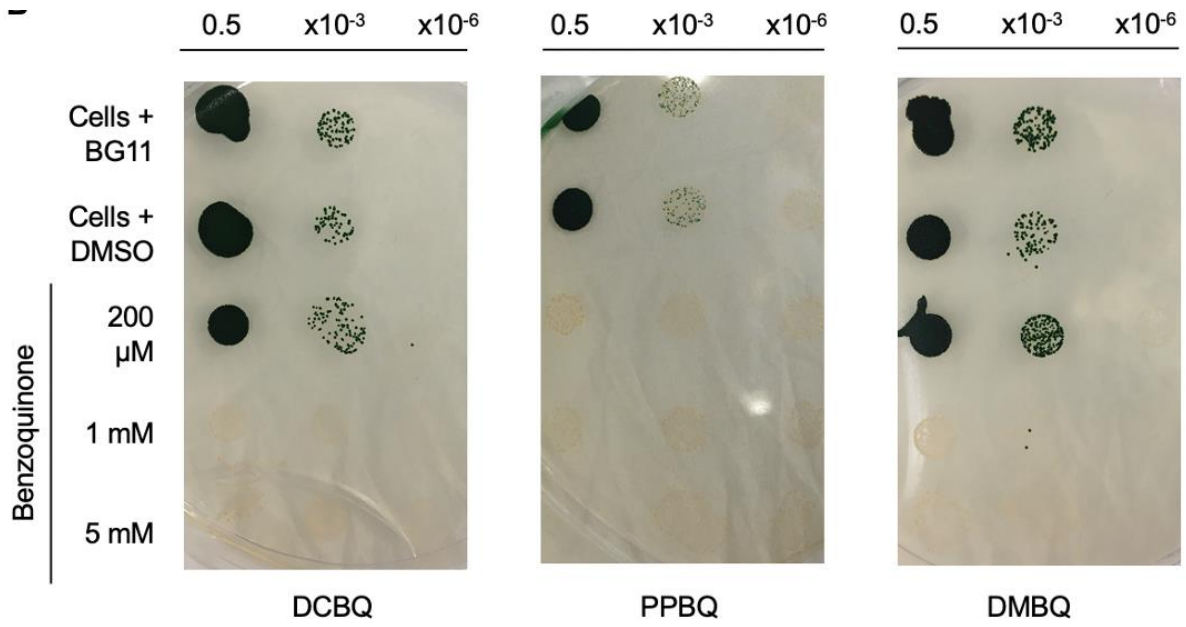

SI Figure 31 - Cytotoxicity spot assays.
Cytotoxicity spot assays to determine the effect of addition of exogenous electron mediators on the growth of wild-type *Synechocystis* cells. Benzoquinones tested: 2,6-dichloro-p-benzoquinone (DCBQ), phenyl-1,4-quinone (PPBQ), 2,6-dimethyl-p-benzoquinone (DMBQ). Cells (5 nmol Chl *a*) were incubated with the mediators at different concentrations for 24 h under 50 $\mu mol_{photons}\ m^{-2}\ s^{-1}$ white light. The cells were resuspended in BG11 and their concentration standardized to an OD_{750} of 0.5. Serial dilutions were prepared, spotted on agar and incubated for 1 week. Cytotoxicity spot assay controls: Cells in BG11 (no mediator), and cells in BG11 with 5 % (v/v) DMSO (no mediator). All data show was from a single representative plate from 3 biological replicates.

8. Chemical Diagrams and Mid-Point Potentials

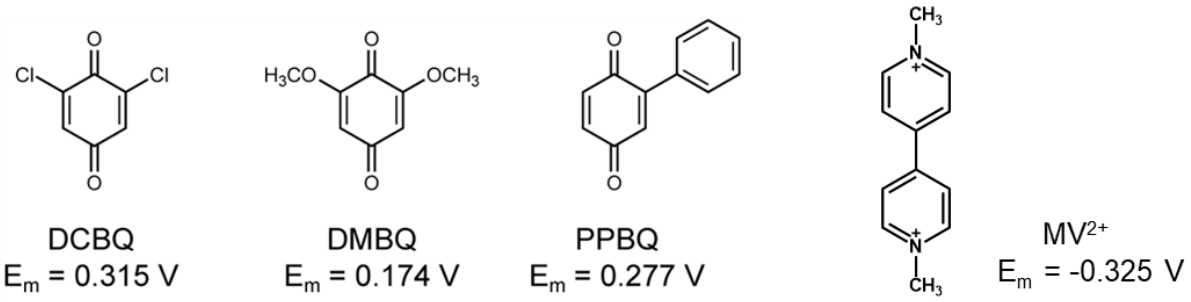

SI Figure 32 – Chemical Structures.

Chemical structures and mid-point potentials of electron mediators used in this study Mediators: 2,6-dichloro-1,4-benzoquinone (DCBQ), phenyl-1,4-quinone (PPBQ), 2,6-dimethyl-p-benzoquinone (DMBQ), and methyl viologen (MV^{2+}). Mid-point potentials (E_m) from the literature versus SHE and at pH 7.[90,91]

Tabulated Lifetimes

Table 3 TA lifetimes (τ) of multiple biological replicates (n = 8) of wild-type cells (SI Figure 2 - Cell replicates.)

Value	τ_1 [fs]	τ_2 [fs]	τ_3 [fs]
Mean	2047.95	4547.56	20803.8
Median	2040.65	4328.63	20783.1
Standard Deviation	327.149	1296.16	2700.56

Table 4 TA lifetimes (τ_q in fs) of wild-type cells with different concentrations of DCBQ added (n = 5) (Figure 2C)

	Concentration of DCBQ added (mM)			
Value	**1**	**2**	**4**	**5**
Mean	21903.9	16613.7	15510.8	11603.7
Median	22369.9	16630.9	15046.5	12600.7
Standard Deviation	3934.5	3813.82	5258.37	5730.34

Table 5 TA lifetimes (τ) of PSI-less cells and PSI-less cells with 1 mM DCBQ added (SI Figure 18 - Analysis of PSI-Less cells in the presence of DCBQ.)

Additive	n	Value	τ_1 [ps]	τ_2 [ps]
-	4	Mean	74.1037	1001.57
		Median	70.4831	997.921
		Standard Deviation	13.6584	381.003
DMBQ 1 mM	4	Mean	52.8946	1260.84
		Median	53.6296	1452
		Standard Deviation	7.10907	870.196

Table 6 TA lifetimes (τ) of isolated PSI and PSI with different concentrations of DCBQ added (SI Figure 17 - Analysis of isolated PSI proteins in the presence of DCBQ.)

Additive	n	Value	τ_1 [ps]	τ_2 [ps]
-	4	Mean	3.25958	24.4735
		Median	3.21766	22.0906
		Standard Deviation	0.293787	5.59445
DMBQ 50 uM	3	Mean	3.16017	19.3718
		Median	3.21141	19.7144
		Standard Deviation	0.235097	2.22661
DCBQ 200 uM	3	Mean	3.24498	17.7529
		Median	3.26468	19.5854
		Standard Deviation	0.241729	4.56605
DCBQ 1 mM	3	Mean	17.7529	2.91984
		Median	19.5854	2.76074
		Standard Deviation	4.56605	0.496354

Table 7 TA lifetimes (τ) of isolated PSII and PSII with 2 mM DCBQ added (SI Figure 19 - Analysis of isolated PSII in the presence of DCBQ.)

Additive	n	Value	τ_1 [ps]	τ_2 [ps]
-	3	Mean	23.1305	986.478
		Median	20.7013	806.422
		Standard Deviation	9.94922	936.567
DMBQ 2 mM	3	Mean	12.1592	1822.44
		Median	11.622	1998
		Standard Deviation	2.26026	781.618

Table 8 TA lifetimes (τ) of PSII-less cells with different concentrations of DCBQ added (SI Figure 18 - Analysis of PSI-Less cells in the presence of DCBQ.)

Additive	n	Value	τ_1 [ps]	τ_2 [ps]	τ_3 [ps]
-	5	Mean	1.37515	4.72576	33.3424
		Median	0.895146	4.29005	39.4114
		Standard Deviation	1.2489	1.32719	9.14994
DMBQ 1 mM	3	Mean	2.02068	3.67077	20.5342
		Median	1.723	3.75088	16.8731
		Standard Deviation	0.60698	0.360788	9.86783
DCBQ 5 mM	3	Mean	1.93172	3.20486	10.3788
		Median	2.60633	3.16679	10.0543
		Standard Deviation	1.24059	1.21283	2.65016

Table 9 TA lifetimes (τ) of wild-type cells with different concentrations of benzoquinone and benzoquinone with DCMU added (Figure 2D & SI Figure 15 – Lifetimes with different benzoquinones and DCMU combinations.)

Additive(s)	n	Value	$\tau_{quinone}/\tau_{cell}$ [ps]
DCBQ 1 mM	5	Mean	0.526043
		Median	0.494251
		Standard Deviation	0.19329
DMBQ 1 mM	5	Mean	1.22641
		Median	1.19472
		Standard Deviation	0.361439
PPBQ 1 mM	5	Mean	1.04763
		Median	1.03462
		Standard Deviation	0,438686
DCMU & DCBQ each 1 mM	4	Mean	0.551711
		Median	0.636816
		Standard Deviation	0.224779
DCMU & DMBQ each 1 mM	4	Mean	0.789561
		Median	0.917867
		Standard Deviation	0.197384
DCMU & PPBQ each 1 mM	4	Mean	0.944083
		Median	0.904805
		Standard Deviation	0.281095

Table 10 TSCPC lifetimes of isolated PSII (SI Figure 28 - TCSPC analysis of biological samples treated with DCBQ or DCMU.)

Replicate number	Sample	Addition	Concentration	Illumination	Measurement	Lifetime τ_1	Lifetime τ_2
1	PSII	DCMU	-	470 nm	680 nm	4.67	1.05
2	PSII	DCMU	-	470 nm	680 nm	4.41	1.04
2	PSII	DCMU	-	470 nm	680 nm	4.21	1.09
1	PSII	-	-	470 nm	680 nm	3.40	1.40
1	PSII	-	-	470 nm	680 nm	3.20	1.20
1	PSII	-	-	470 nm	680 nm	3.51	1.04
1	PSII	DCBQ	10 uM	470 nm	680 nm	3.04	1.01
1	PSII	DCBQ	50 uM	470 nm	680 nm	1.77	0.29
2	PSII	DCBQ	50 uM	470 nm	680 nm	3.37	0.95
2	PSII	DCBQ	50 uM	470 nm	680 nm	2.77	0.79
1	PSII	DCBQ	200 uM	470 nm	680 nm	1.23	0.24

2	PSII	DCBQ	200 uM	470 nm	680 nm	2.14	0.46
2	PSII	DCBQ	200 uM	470 nm	680 nm	1.65	0.35
1	PSII	DCBQ	1 mM	470 nm	680 nm	1.39	0.16
1	PSII	DCBQ	1 mM	470 nm	680 nm	1.38	0.21

Table 11 TCSPC lifetimes of wild-type cells (SI Figure 28 - TCSPC analysis of biological samples treated with DCBQ or DCMU.)

Excitation 407 nm

Replicate number	Addition	Concentration	Illumination	Measurement	Lifetime τ_1	Lifetime τ_2
1	DCMU	1 mM	407 nm	680 nm	1.57	0.52
2	DCMU	1 mM	407 nm	680 nm	1.6	0.48
3	DCMU	1 mM	407 nm	680 nm	1.52	0.62
1	-	-	407 nm	680 nm	1.44	0.55
2	-	-	407 nm	680 nm	1.45	0.37
1	DCBQ	200 uM	407 nm	680 nm	1.24	0.42
2	DCBQ	200 uM	407 nm	680 nm	1.33	0.51
3	DCBQ	200 uM	407 nm	680 nm	1.26	0.38
1	DCBQ	1 mM	407 nm	680 nm	1.15	0.39
2	DCBQ	1 mM	407 nm	680 nm	1.19	0.43
3	DCBQ	1 mM	407 nm	680 nm	1.21	0.24

Excitation 470 nm

Replicate number	Addition	Concentration	Illumination	Measurement	Lifetime τ_1	Lifetime τ_2
1	DCMU	1 mM	470 nm	680 nm	2.15	0.70
1	-	-	470 nm	680 nm	2.03	0.62
2	-	-	470 nm	680 nm	2.01	0.55
1	DCBQ	1 mM	470 nm	680 nm	1.96	0.41
1	DCBQ	5 mM	470 nm	680 nm	1.84	0.32

Table 12 TCSPC lifetimes of control samples (SI Figure 29 - TCSPC controls.)

Replicate number	Addition	Concentration	Illumination	Measurement	Lifetime τ_1	Lifetime τ_2
1	DMSO	5%	407 nm	680 nm	1.39	0.38
1	DMSO	10%	407 nm	680 nm	1.42	0.37
1	DMSO	0.2%	470 nm	680 nm	1.98	0.59
1	DMSO	1%	470 nm	680 nm	2.00	0.58
2	DMSO	5%	470 nm	680 nm	1.80	0.62

References

1. Schreiber, U., Endo, T., Mi, H. & Asada, K. Quenching analysis of chlorophyll fluorescence by the saturation pulse method: Particular aspects relating to the study of eukaryotic algae and cyanobacteria. *Plant Cell Physiol* (1995) doi:10.1093/oxfordjournals.pcp.a078833.
2. Hinrichsen, T. F. *et al.* Long-lived and disorder-free charge transfer states enable endothermic charge separation in efficient non-fullerene organic solar cells. doi:10.1038/s41467-020-19332-5.
3. Mersch, D. *et al.* Wiring of Photosystem II to Hydrogenase for Photoelectrochemical Water Splitting. *J Am Chem Soc* **137**, 8541–8549 (2015).
4. Çoruh, O. *et al.* Cryo-EM structure of a functional monomeric Photosystem I from Thermosynechococcus elongatus reveals red chlorophyll cluster. *Commun Biol* **4**, 304 (2021).
5. Shen, G., Boussiba, S. & Vermaas, W. F. J. Synechocystis sp PCC 6803 Strains Lacking Photosystem I and Phycobilisome Function. *Plant Cell* **5**, 1853 (2007).
6. Ermakova-Gerdes, S., Yu, Z. & Vermaas, W. Targeted random mutagenesis to identify functionally important residues in the D2 protein of photosystem II in Synechocystis sp. strain PCC 6803. *J Bacteriol* **183**, 145–154 (2001).
7. Lea-Smith, D. J. *et al.* Phycobilisome-Deficient Strains of Synechocystis sp PCC 6803 Have Reduced Size and Require Carbon-Limiting Conditions to Exhibit Enhanced Productivity. *Plant Physiol* **165**, 705–714 (2014).
8. Berera, R., van Grondelle, R. & Kennis, J. T. M. Ultrafast transient absorption spectroscopy: Principles and application to photosynthetic systems. *Photosynth Res* **101**, 105–118 (2009).
9. Zhang, J. Z. *et al.* Photoelectrochemistry of Photosystem II in Vitro vs in Vivo. *J Am Chem Soc* **140**, 6–9 (2018).
10. Zamzam, N. *et al.* Femtosecond visible transient absorption spectroscopy of chlorophyll-f-containing photosystem II. *Proc Natl Acad Sci U S A* **117**, 23158–23164 (2020).
11. *Photosystem I*. vol. 24 (Springer Netherlands, 2006).
12. Karapetyan, N. V., Holzwarth, A. R. & Rögner, M. The photosystem I trimer of cyanobacteria: molecular organization, excitation dynamics and physiological significance. *FEBS Lett* **460**, 395–400 (1999).
13. Croce, R., Zucchelli, G., Garlaschi, F. M. & Jennings, R. C. A thermal broadening study of the antenna chlorophylls in PSI- 200, LHCI, and PSI core. *Biochemistry* **37**, 17355–17360 (1998).
14. Karapetyan, N. V. *et al.* Long-wavelength chlorophylls in photosystem I of cyanobacteria: Origin, localization, and functions. *Biochemistry (Moscow) 2014 79:3* **79**, 213–220 (2014).
15. Molotokaite, E. *et al.* Trapping Dynamics in Photosystem I-Light Harvesting Complex i of Higher Plants Is Governed by the Competition between Excited State Diffusion from Low Energy States and Photochemical Charge Separation. *Journal of Physical Chemistry B* **121**, 9816–9830 (2017).
16. Russo, M., Casazza, A. P., Cerullo, G., Santabarbara, S. & Maiuri, M. Ultrafast excited state dynamics in the monomeric and trimeric photosystem I core complex of Spirulina platensis probed by two-dimensional electronic spectroscopy. *J Chem Phys* **156**, 164202 (2022).
17. Akhtar, P. *et al.* Two-Dimensional Electronic Spectroscopy of a Minimal Photosystem I Complex Reveals the Rate of Primary Charge Separation. *J Am Chem Soc* **143**, 14601–14612 (2021).
18. Shelaev, I. V. *et al.* Femtosecond primary charge separation in Synechocystis sp. PCC 6803 photosystem I. *Biochimica et Biophysica Acta (BBA) - Bioenergetics* **1797**, 1410–1420 (2010).
19. Cherepanov, D. A. *et al.* Mechanism of adiabatic primary electron transfer in photosystem I: Femtosecond spectroscopy upon excitation of reaction center in the far-red edge of the QY band. *Biochimica et Biophysica Acta (BBA) - Bioenergetics* **1858**, 895–905 (2017).
20. Hastings, G., Reed, L. J., Lin, S. & Blankenship, R. E. Excited state dynamics in photosystem I: effects of detergent and excitation wavelength. *Biophys J* **69**, 2044–2055 (1995).
21. Lee, Y., Gorka, M., Golbeck, J. H. & Anna, J. M. Ultrafast Energy Transfer Involving the Red Chlorophylls of Cyanobacterial Photosystem i Probed through Two-Dimensional Electronic Spectroscopy. *J Am Chem Soc* **140**, 11631–11638 (2018).
22. Anna, J. M., Ostroumov, E. E., Maghlaoui, K., Barber, J. & Scholes, G. D. Two-dimensional electronic spectroscopy reveals ultrafast downhill energy transfer in photosystem i trimers of the

cyanobacterium thermosynechococcus elongatus. *Journal of Physical Chemistry Letters* **3**, 3677–3684 (2012).
23. Mülle, M. G., Niklas, J., Lubitz, W. & Holzwarth, A. R. Ultrafast Transient Absorption Studies on Photosystem I Reaction Centers from Chlamydomonas reinhardtii. 1. A New Interpretation of the Energy Trapping and Early Electron Transfer Steps in Photosystem I. *Biophys J* **85**, 3899–3922 (2003).
24. Melkozernov, A. N. *et al.* Specific Mutation Near the Primary Donor in Photosystem I from Chlamydomonas reinhardtii Alters the Trapping Time and Spectroscopic Properties of P700†. *Biochemistry* **36**, 2898–2907 (1997).
25. Russo, M. *et al.* Ultrafast excited-state dynamics in land plants Photosystem I core and whole supercomplex under oxidised electron donor conditions. *Photosynth Res* **144**, 221–233 (2020).
26. Slavov, C., Ballottari, M., Morosinotto, T., Bassi, R. & Holzwarth, A. R. Trap-Limited Charge Separation Kinetics in Higher Plant Photosystem I Complexes. *Biophys J* **94**, 3601–3612 (2008).
27. Santabarbara, S., Tibiletti, T., Remelli, W. & Caffarri, S. Kinetics and heterogeneity of energy transfer from light harvesting complex II to photosystem I in the supercomplex isolated from Arabidopsis. *Physical Chemistry Chemical Physics* **19**, 9210–9222 (2017).
28. Akhtar, P. *et al.* Excitation energy transfer between Light-harvesting complex II and Photosystem I in reconstituted membranes. *Biochimica et Biophysica Acta (BBA) - Bioenergetics* **1857**, 462–472 (2016).
29. Van Stokkum, I. H. M., Larsen, D. S. & Van Grondelle, R. Global and target analysis of time-resolved spectra. *Biochim Biophys Acta Bioenerg* **1657**, 82–104 (2004).
30. Dorlhiac, G. F., Fare, C. & van Thor, J. J. PyLDM - An open source package for lifetime density analysis of time-resolved spectroscopic data. *PLoS Comput Biol* **13**, e1005528 (2017).
31. van Stokkum, I. H. M., Larsen, D. S. & van Grondelle, R. Global and target analysis of time-resolved spectra. *Biochimica et Biophysica Acta (BBA) - Bioenergetics* **1657**, 82–104 (2004).
32. Berera, R., van Grondelle, R. & Kennis, J. T. M. Ultrafast transient absorption spectroscopy: Principles and application to photosynthetic systems. *Photosynthesis Research* vol. 101 105–118 Preprint at https://doi.org/10.1007/s11120-009-9454-y (2009).
33. Mülle, M. G., Niklas, J., Lubitz, W. & Holzwarth, A. R. Ultrafast Transient Absorption Studies on Photosystem I Reaction Centers from Chlamydomonas reinhardtii. 1. A New Interpretation of the Energy Trapping and Early Electron Transfer Steps in Photosystem I. *Biophys J* **85**, 3899–3922 (2003).
34. Sugiura, M. & Inoue, Y. Highly purified thermo-stable oxygen-evolving photosystem II core complex from the thermophilic cyanobacterium Synechococcus elongatus having His-tagged CP43. *Plant Cell Physiol* **40**, 1219–1231 (1999).
35. El-Mohsnawy, E. *et al.* Structure and Function of Intact Photosystem 1 Monomers from the Cyanobacterium Thermosynechococcus elongatus. *Biochemistry* **49**, 4740–4751 (2010).
36. Komenda, J. & Sobotka, R. Chlorophyll-binding subunits of photosystem I and II: Biosynthesis, chlorophyll incorporation and assembly. *Adv Bot Res* **91**, 195–223 (2019).
37. Boehm, M. *et al.* Investigating the Early Stages of Photosystem II Assembly in Synechocystis sp. PCC 6803: ISOLATION OF CP47 AND CP43 COMPLEXES. *Journal of Biological Chemistry* **286**, 14812–14819 (2011).
38. Förster, T. Zwischenmolekulare Energiewanderung und Fluoreszenz. *Ann Phys* **437**, 55–75 (1948).
39. Scholes, G. D. Long-Range Resonance Energy Transfer in Molecular Systems. *https://doi.org/10.1146/annurev.physchem.54.011002.103746* **54**, 57–87 (2003).
40. Beljonne, D., Curutchet, C., Scholes, G. D. & Silbey, R. J. Beyond förster resonance energy transfer in biological and nanoscale systems. *Journal of Physical Chemistry B* **113**, 6583–6599 (2009).
41. Dexter, D. L. A Theory of Sensitized Luminescence in Solids. *J Chem Phys* **21**, 836 (2004).
42. Köhler, A. & Bässler, H. *Electronic Processes in Organic Semiconductors*.
43. Laquai, F., Park, Y. S., Kim, J. J. & Basché, T. Excitation Energy Transfer in Organic Materials: From Fundamentals to Optoelectronic Devices. *Macromol Rapid Commun* **30**, 1203–1231 (2009).
44. Klessinger, M. & Michl, J. Excited States and Photo-Chemistry of Organic Molecules, Revised and Improved English-Language Edition. 537 (1995).
45. Vogel, P. & Houk, K. Theory reactivity and mechanisms in modern synthesis. 1382 (2019).

46. Marcus, R. A. On the Theory of Oxidation-Reduction Reactions Involving Electron Transfer. I. *J Chem Phys* **24**, 966 (2004).
47. Longatte, G. *et al.* Investigation of photocurrents resulting from a living unicellular algae suspension with quinones over time. *Chem Sci* **9**, 8271–8281 (2018).
48. Longatte, G. *et al.* Evaluation of photosynthetic electrons derivation by exogenous redox mediators. *Biophys Chem* **205**, 1–8 (2015).
49. Fu, H.-Y. *et al.* Redesigning the QA binding site of Photosystem II allows reduction of exogenous quinones. *Nat Commun* **8**, 15274 (2017).
50. Longatte, G., Rappaport, F., Wollman, F.-A., Guille-Collignon, M. & Lemaître, F. Mechanism and analyses for extracting photosynthetic electrons using exogenous quinones – what makes a good extraction pathway? *Photochemical & Photobiological Sciences* **15**, 969–979 (2016).
51. Trebst, A. The three-dimensional structure of the herbicide binding niche on the reaction center polypeptides of photosystem ii. *Zeitschrift fur Naturforschung - Section C Journal of Biosciences* **42**, 742–750 (1987).
52. Bennett, T. *et al.* Elucidating the role of methyl viologen as a scavenger of photoactivated electrons from photosystem I under aerobic and anaerobic conditions. *Physical Chemistry Chemical Physics* **18**, 8512–8521 (2016).
53. Jones, R. W. & Garland, P. B. Sites and specificity of the reaction of bipyridylium compounds with anaerobic respiratory enzymes of Escherichia coli. Effects of permeability barriers imposed by the cytoplasmic membrane. *Biochemical Journal* **164**, 199 (1977).
54. Lawrence, J. M. *et al.* Synthetic biology and bioelectrochemical tools for electrogenetic system engineering. *Sci Adv* **8**, 5091 (2022).
55. Sayegh, A. *et al.* Finding Adapted Quinones for Harvesting Electrons from Photosynthetic Algae Suspensions. *ChemElectroChem* **8**, 2968–2978 (2021).
56. Kohler, A. & Bassler, H. *The Electronic Structure of Organic Semiconductors*. *Wiley-VCH Verlag GmbH & Co. KGaA* vol. 1 (2015).
57. Marcus, R. A. & Sutin, N. Electron transfers in chemistry and biology. *BBA Reviews On Bioenergetics* vol. 811 265–322 Preprint at https://doi.org/10.1016/0304-4173(85)90014-X (1985).
58. Watanabe, M., Iwai, M., Narikawa, R. & Ikeuchi, M. Is the Photosystem II Complex a Monomer or a Dimer? *Plant Cell Physiol* **50**, 1674–1680 (2009).
59. Young, I. D. *et al.* Structure of photosystem II and substrate binding at room temperature. *Nature* **540**, 453–457 (2016).
60. Boekema, E. J. *et al.* Evidence for a trimeric organization of the photosystem I complex from the thermophilic cyanobacterium *Synechococcus* sp. *FEBS Lett* **217**, 283–286 (1987).
61. Ivanov, A. G. *et al.* Iron Deficiency in Cyanobacteria Causes Monomerization of Photosystem I Trimers and Reduces the Capacity for State Transitions and the Effective Absorption Cross Section of Photosystem I in Vivo. *Plant Physiol* **141**, 1436–1445 (2006).
62. Kłodawska, K. *et al.* Elevated Growth Temperature Can Enhance Photosystem I Trimer Formation and Affects Xanthophyll Biosynthesis in Cyanobacterium Synechocystis sp. PCC6803 Cells. *Plant Cell Physiol* **56**, 558–571 (2015).
63. Kouřil, R., van Oosterwijk, N., Yakushevska, A. E. & Boekema, E. J. Photosystem I: a search for green plant trimers. *Photochemical & Photobiological Sciences* **4**, 1091 (2005).
64. Gardian, Z. *et al.* Organisation of Photosystem I and Photosystem II in red alga Cyanidium caldarium: Encounter of cyanobacterial and higher plant concepts. *Biochimica et Biophysica Acta (BBA) - Bioenergetics* **1767**, 725–731 (2007).
65. Veith, T. & Büchel, C. The monomeric photosystem I-complex of the diatom Phaeodactylum tricornutum binds specific fucoxanthin chlorophyll proteins (FCPs) as light-harvesting complexes. *Biochimica et Biophysica Acta (BBA) - Bioenergetics* **1767**, 1428–1435 (2007).
66. Heinemeyer, J., Eubel, H., Wehmhöner, D., Jänsch, L. & Braun, H.-P. Proteomic approach to characterize the supramolecular organization of photosystems in higher plants. *Phytochemistry* **65**, 1683–92 (2004).
67. Jordan, P. *et al.* Three-dimensional structure of cyanobacterial photosystem I at 2.5 Å resolution. *Nature* **411**, 909–917 (2001).

68. Fromme, P., Jordan, P. & Krauß, N. Structure of photosystem I. *Biochimica et Biophysica Acta (BBA) - Bioenergetics* **1507**, 5–31 (2001).
69. Fromme, P., Schubert, W.-D. & Krauß, N. Structure of Photosystem I: Suggestions on the docking sites for plastocyanin, ferredoxin and the coordination of P700. *Biochimica et Biophysica Acta (BBA) - Bioenergetics* **1187**, 99–105 (1994).
70. Stirbet, A. Excitonic connectivity between photosystem II units: What is it, and how to measure it? *Photosynthesis Research* vol. 116 189–214 Preprint at https://doi.org/10.1007/s11120-013-9863-9 (2013).
71. Mirkovic, T. *et al.* Light absorption and energy transfer in the antenna complexes of photosynthetic organisms. *Chemical Reviews* vol. 117 249–293 Preprint at https://doi.org/10.1021/acs.chemrev.6b00002 (2017).
72. Dods, R. *et al.* Ultrafast structural changes within a photosynthetic reaction centre. *Nature* **589**, 310–314 (2021).
73. Ma, F., Romero, E., Jones, M. R., Novoderezhkin, V. I. & van Grondelle, R. Both electronic and vibrational coherences are involved in primary electron transfer in bacterial reaction center. *Nat Commun* **10**, 933 (2019).
74. Zouni, A. *et al.* Crystal structure of photosystem II from Synechococcus elongatus at 3.8 Å resolution. *Nature* **409**, 739–743 (2001).
75. Clifford, E. R. *et al.* Phenazines as model low-midpoint potential electron shuttles for photosynthetic bioelectrochemical systems. *Chem Sci* **12**, 3328–3338 (2021).
76. Zhang, J. Z. & Reisner, E. Advancing photosystem II photoelectrochemistry for semi-artificial photosynthesis. *Nat Rev Chem* **4**, 6–21 (2020).
77. Sokol, K. P. *et al.* Rational wiring of photosystem II to hierarchical indium tin oxide electrodes using redox polymers. *Energy Environ Sci* **9**, 3698–3709 (2016).
78. Saper, G. *et al.* Live cyanobacteria produce photocurrent and hydrogen using both the respiratory and photosynthetic systems. *Nat Commun* **9**, 2168 (2018).
79. Shlosberg, Y. *et al.* NADPH performs mediated electron transfer in cyanobacterial-driven bio-photoelectrochemical cells. *iScience* **24**, 101892 (2021).
80. Kato, M., Cardona, T., Rutherford, a W. & Reisner, E. Photoelectrochemical Water Oxidation with Photosystem II Integrated in a Mesoporous Indium Tin Oxide Electrode. *J Am Chem Soc* **134**, 8332–8335 (2012).
81. Ulas, G. & Brudvig, G. W. Redirecting Electron Transfer in Photosystem II from Water to Redox-Active Metal Complexes. *J Am Chem Soc* **133**, 13260–13263 (2011).
82. Sugiura, M. & Inoue, Y. Highly Purified Thermo-Stable Oxygen-Evolving Photosystem II Core Complex from the Thermophilic Cyanobacterium Synechococcus elongatus Having His-Tagged CP43. *Plant Cell Physiol* **40**, 1219–1231 (1999).
83. Onishi, A., Aikawa, S., Kondo, A. & Akimoto, S. Energy transfer in Anabaena variabilis filaments adapted to nitrogen-depleted and nitrogen-enriched conditions studied by time-resolved fluorescence. *Photosynth Res* **133**, 317–326 (2017).
84. Chukhutsina, V., Bersanini, L., Aro, E.-M., van Amerongen, H. & van Amerongen, H. Cyanobacterial flv4-2 Operon-Encoded Proteins Optimize Light Harvesting and Charge Separation in Photosystem II. *Mol Plant* **8**, 747–761 (2015).
85. Mascoli, V., Bersanini, L. & Croce, R. Far-red absorption and light-use efficiency trade-offs in chlorophyll f photosynthesis. *Nat Plants* **6**, 1044–1053 (2020).
86. Bar-Eyal, L. *et al.* An easily reversible structural change underlies mechanisms enabling desert crust cyanobacteria to survive desiccation. *Biochim Biophys Acta Bioenerg* **1847**, 1267–1273 (2015).
87. Lavergne, J. Improved UV-visible spectra of the S-transitions in the photosynthetic oxygen-evolving system. *Biochimica et Biophysica Acta (BBA) - Bioenergetics* **1060**, 175–188 (1991).
88. Lea-Smith, D. J., Bombelli, P., Vasudevan, R. & Howe, C. J. Photosynthetic, respiratory and extracellular electron transport pathways in cyanobacteria. *Biochim Biophys Acta Bioenerg* **1857**, 247–255 (2016).
89. Sétif, P., Boussac, A. & Krieger-Liszkay, A. Near-infrared in vitro measurements of photosystem I cofactors and electron-transfer partners with a recently developed spectrophotometer. *Photosynth Res* **142**, 307–319 (2019).

90. Longatte, G. *et al.* Investigation of photocurrents resulting from a living unicellular algae suspension with quinones over time. *Chem Sci* **9**, 8271–8281 (2018).
91. O'Reilly, J. E. Oxidation-reduction potential of the ferro-ferricyanide system in buffer solutions. *Biochimica et Biophysica Acta (BBA) - Bioenergetics* **292**, 509–515 (1973).